NASA/TM—2019-220163

On the Use of Optimization Techniques for Turbulence Model Calibration

Dennis A. Yoder
Glenn Research Center, Cleveland, Ohio

Paul D. Orkwis
University of Cincinnati, Cincinnati, Ohio

May 2019

NASA STI Program . . . in Profile

Since its founding, NASA has been dedicated to the advancement of aeronautics and space science. The NASA Scientific and Technical Information (STI) Program plays a key part in helping NASA maintain this important role.

The NASA STI Program operates under the auspices of the Agency Chief Information Officer. It collects, organizes, provides for archiving, and disseminates NASA's STI. The NASA STI Program provides access to the NASA Technical Report Server—Registered (NTRS Reg) and NASA Technical Report Server—Public (NTRS) thus providing one of the largest collections of aeronautical and space science STI in the world. Results are published in both non-NASA channels and by NASA in the NASA STI Report Series, which includes the following report types:

- TECHNICAL PUBLICATION. Reports of completed research or a major significant phase of research that present the results of NASA programs and include extensive data or theoretical analysis. Includes compilations of significant scientific and technical data and information deemed to be of continuing reference value. NASA counter-part of peer-reviewed formal professional papers, but has less stringent limitations on manuscript length and extent of graphic presentations.

- TECHNICAL MEMORANDUM. Scientific and technical findings that are preliminary or of specialized interest, e.g., "quick-release" reports, working papers, and bibliographies that contain minimal annotation. Does not contain extensive analysis.

- CONTRACTOR REPORT. Scientific and technical findings by NASA-sponsored contractors and grantees.

- CONFERENCE PUBLICATION. Collected papers from scientific and technical conferences, symposia, seminars, or other meetings sponsored or co-sponsored by NASA.

- SPECIAL PUBLICATION. Scientific, technical, or historical information from NASA programs, projects, and missions, often concerned with subjects having substantial public interest.

- TECHNICAL TRANSLATION. English-language translations of foreign scientific and technical material pertinent to NASA's mission.

For more information about the NASA STI program, see the following:

- Access the NASA STI program home page at http://www.sti.nasa.gov

- E-mail your question to help@sti.nasa.gov

- Fax your question to the NASA STI Information Desk at 757-864-6500

- Telephone the NASA STI Information Desk at 757-864-9658

- Write to:
  NASA STI Program
  Mail Stop 148
  NASA Langley Research Center
  Hampton, VA 23681-2199

NASA/TM—2019-220163

On the Use of Optimization Techniques for Turbulence Model Calibration

Dennis A. Yoder
Glenn Research Center, Cleveland, Ohio

Paul D. Orkwis
University of Cincinnati, Cincinnati, Ohio

National Aeronautics and
Space Administration

Glenn Research Center
Cleveland, Ohio 44135

May 2019

Acknowledgments

This research was sponsored by NASA's Transformational Tools and Technologies (TTT) Project of the Transformative Aeronautics Concepts Program under the Aeronautics Research Mission Directorate.

Level of Review: This material has been technically reviewed by technical management.

Available from

NASA STI Program
Mail Stop 148
NASA Langley Research Center
Hampton, VA 23681-2199

National Technical Information Service
5285 Port Royal Road
Springfield, VA 22161
703-605-6000

This report is available in electronic form at http://www.sti.nasa.gov/ and http://ntrs.nasa.gov/

On the Use of Optimization Techniques for Turbulence Model Calibration

Dennis A. Yoder
National Aeronautics and Space Administration
Glenn Research Center
Cleveland, Ohio 44135

Paul D. Orkwis
University of Cincinnati
Cincinnati, Ohio 45221

Abstract

This article discusses the use of numerical optimization procedures to aid in the calibration of turbulence model coefficients. Such methods would increase the rigor and repeatability of the calibration procedure by requiring clearly defined and objective optimization metrics, and could be used to identify unique combinations of coefficient values for specific flow problems. The approach is applied to the re-calibration of an explicit algebraic Reynolds stress model for the incompressible planar mixing layer using the Nelder-Mead simplex algorithm and a micro-genetic algorithm with minimally imposed constraints. Three composite fitness functions, each based upon the error in the mixing layer growth rate and the normal and shear components of the Reynolds stresses, are investigated. The results demonstrate a significant improvement in the target objectives through the adjustment of three pressure-strain coefficients. Adjustments of additional coefficients provide little further benefit. Issues regarding the effectiveness of the fitness functions and the efficiency of the optimization algorithms are also discussed.

Nomenclature

b_{ij}	turbulence anisotropy tensor, $b_{ij} = \left(-\tau_{ij}^{T} - \frac{2}{3}\bar{\rho}k\delta_{ij}\right)/2\bar{\rho}k$
C_1^0, C_1^1, C_2, C_3, C_4	pressure strain coefficients
C_μ	eddy viscosity coefficient
$\mathcal{D}$	diffusion of turbulent kinetic energy, $\mathcal{D} = \mathcal{D}_{kk}/2$
$\mathcal{D}_{ij}$	diffusion of turbulent stress
e	internal energy
f_μ, f_1, f_2	damping functions in $k-\epsilon$ eddy viscosity model
h	enthalpy
k	turbulent kinetic energy
L_1^0, L_1^1, L_2, L_3, L_4	scalar terms in algebraic stress model
L_k, L_ϵ	near-wall terms in $k-\epsilon$ eddy viscosity model
P	pressure
$\mathcal{P}$	production of turbulent kinetic energy, $\mathcal{P} = \tau_{ij}^{T}\widetilde{u}_{i,j}$
$\mathcal{P}_{ij}$	production of turbulent stress
Pr	Prandtl number
q_j	heat flux vector
$R_{i,j}$	rotation rate tensor, $R_{ij} = (u_{i,j} - u_{j,i})/2$
$S_{i,j}$	strain rate tensor, $S_{ij} = (u_{i,j} + u_{j,i})/2$
t	time

u_j	velocity vector
U^*	self-similar velocity profile, $U^* = (\tilde{u} - \tilde{u}_2)/(\tilde{u}_1 - \tilde{u}_2)$
x	streamwise coordinate
x_j	spatial coordinate vector
x_0	virtual origin of mixing layer
y	transverse coordinate
$y_{0.5}$	center of the mixing layer, where $U^* = 0.5$

Subscripts

1	high-speed side of mixing layer
2	low-speed side of mixing layer
L	laminar
T	turbulent

Conventions

$''$	Favre fluctuation
$\sim$	Favre average
$-$	Reynolds average

Symbols

δ_ω	mixing layer vorticity thickness, $\delta_\omega = (\tilde{u}_1 - \tilde{u}_2)/(\partial\tilde{u}/\partial y)_{\max}$
δ_{ij}	Kronecker delta
ϵ	turbulent dissipation rate
γ_2	switch for algebraic stress diffusion approximation
η	similarity variable, $\eta = \sigma(y - y_{0.5})/(x - x_0)$
η_1	flow invariant, $(k/\epsilon)^2 \widetilde{S}_{ij}\widetilde{S}_{ji}$
η_2	flow invariant, $(k/\epsilon)^2 \widetilde{R}_{ij}\widetilde{R}_{ji}$
μ	viscosity
ϕ	switch for treatment of production to dissipation ratio
Π_{ij}	pressure-strain correlation tensor
ρ	density
σ	spread rate parameter, $\sigma = \sqrt{\pi}/(d\delta_\omega/dx)$
σ_k, σ_ϵ	diffusion coefficients
τ_{ij}	stress tensor
ξ	interpolation coefficient

Superscripts

D	deviatoric

Acronyms

ABS	error based on peak absolute value
ASM	algebraic stress model
EVM	eddy viscosity model
FANS	Favre-averaged Navier-Stokes
GA	genetic algorithm
HO	hand optimized
LES	large eddy simulation
NM	Nelder-Mead
RANS	Reynolds-averaged Navier-Stokes
RMS	error based on integral root mean square value
RSM	Reynolds stress model
SQR	error based on peak squared value

I. Introduction

Despite growing interest in higher-fidelity methods such as Large Eddy Simulation (LES), turbulence models based on the Reynolds- or Favre-averaged Navier-Stokes (RANS/FANS) equations are still widely used to simulate aerodynamic and propulsion flows due to their relatively low cost and long history of documented successes and known limitations. The averaging procedures used in the formulation of these methods introduce additional unknown correlation terms that must somehow be taken into consideration. The most important of these correlation terms are aptly referred to as the turbulent heat flux vector and turbulent stress tensor.

Turbulence models of varying degrees of sophistication have been developed to approximate the behavior of these terms. All of these models introduce closure coefficients that must either be prescribed or calibrated against known data. In order to facilitate this calibration, a series of fundamental cases are typically used to isolate specific terms and coefficients within the model. These same constant coefficient values are then assumed to remain valid across a range of flows, which might not be true.

Numerical optimization techniques have great potential for improving turbulence model calibration. These methods require the specification and quantification of an objective optimization metric, which could be used to more clearly document the calibration process and ensure its repeatability. Furthermore, these methods can be automated to find the best coefficient values within a prescribed range and can be used to determine the best combination of coefficient values. Constraints can be implemented to ensure compliance with relevant physical laws. The use of optimization techniques would therefore provide greater rigor in defining the model and could provide insight into how the coefficient values would need to change in order to simulate more complex flows.

This study investigates the use of numerical optimization techniques in recalibrating turbulence model coefficients within the self-similar region of an incompressible planar mixing layer. Changes to various combinations of coefficients are explored as is the sensitivity to and effectiveness of the objective function. The optimization methods used do not necessarily represent the fastest or most state-of-the-art techniques, but were chosen to demonstrate the feasibility of the approach when applied to the turbulence model equation set. It will be shown that the optimization methods can be used to obtain a better calibration for the turbulent shear stress (and therefore improved mixing) as well as turbulence anisotropy. In addition, this study demonstrates limitations in the current model formulation, particularly with regards to predicting turbulence levels near the edges of the shear layer.

This paper is organized as follows. Section II provides background information regarding the modeled transport equations, a brief summary of how turbulence model coefficients are typically calibrated, and justifications for the use of optimization methods as part of that process. Section III describes the numerical optimization methods chosen for this task, namely the simplex algorithm and genetic algorithm. The numerical methods used in this study are outlined in section IV, the calibration results for the incompressible planar shear layer are presented in section V, and a discussion of the overall findings is contained in section VI.

II. Background

The Favre-averaged form of the Navier-Stokes equations can be written as

$$\frac{\partial \bar{\rho}}{\partial t} + \frac{\partial \bar{\rho}\widetilde{u}_j}{\partial x_j} = 0 \tag{1}$$

$$\frac{\partial \bar{\rho}\widetilde{u}_i}{\partial t} + \frac{\partial}{\partial x_j}\left[\bar{\rho}\widetilde{u}_i\widetilde{u}_j + \bar{P}\delta_{ij} - \left(\tau_{ij}^L + \tau_{ij}^T\right)\right] = 0 \tag{2}$$

$$\frac{\partial}{\partial t}\left[\bar{\rho}\left(\widetilde{e} + \frac{1}{2}\widetilde{u}_i\widetilde{u}_i + k\right)\right] + \frac{\partial}{\partial x_j}\left[\bar{\rho}\widetilde{u}_j\left(\widetilde{h} + \frac{1}{2}\widetilde{u}_i\widetilde{u}_i + k\right) - \widetilde{u}_i\left(\tau_{ij}^L + \tau_{ij}^T\right) + \left(q_j^L + q_j^T\right)\right] = 0 \tag{3}$$

where the laminar stress and heat flux are given by

$$\tau_{ij}^{L} = \mu_{L}\left(\frac{\partial \widetilde{u}_i}{\partial x_j} + \frac{\partial \widetilde{u}_j}{\partial x_i} - \frac{2}{3}\frac{\partial \widetilde{u}_k}{\partial x_k}\delta_{ij}\right) \tag{4}$$

$$q_j^{L} = -\frac{\mu_{L}}{Pr}\frac{\partial \widetilde{h}}{\partial x_j} \tag{5}$$

and the turbulent stress, heat flux, and kinetic energy are defined in terms of the unknown correlations.

$$\tau_{ij}^{T} = -\overline{\rho u_i'' u_j''} \tag{6}$$

$$q_j^{T} = \overline{\rho u_j'' h''} \tag{7}$$

$$\bar{\rho} k = \frac{1}{2}\overline{\rho u_i'' u_i''} \tag{8}$$

The turbulent heat flux is typically modeled using a gradient diffusion approach together with Reynolds[1] analogy between momentum and heat transfer, resulting in an expression that is similar to the laminar contribution.

$$q_j^{T} = -\frac{\mu_{T}}{Pr_{T}}\frac{\partial \widetilde{h}}{\partial x_j} \tag{9}$$

Models for the turbulent stress generally fall into three classes: differential Reynolds stress models (RSMs) which solve transport equations for each of the Reynolds stresses; algebraic Reynolds stress models (ASMs) which are a reduced form of the differential stress models; and eddy viscosity models (EVMs) which relate the turbulent stress to the mean rate of strain through a scalar turbulent viscosity, yet often solve transport equations to obtain the necessary turbulent velocity and length scales.

A differential Reynolds stress model similar to that of Launder, Reece and Rodi,[2] but with a simple gradient diffusion term that is more in-line with the other models to be discussed, can be written as follows.

$$\frac{\partial}{\partial t}\left(-\tau_{ij}^{T}\right) + \frac{\partial}{\partial x_k}\left(-\tau_{ij}^{T}\tilde{u}_k\right) = \mathcal{P}_{ij} + \mathcal{D}_{ij} + \Pi_{ij} - \frac{2}{3}\bar{\rho}\epsilon\delta_{ij} \tag{10}$$

$$\mathcal{P}_{ij} = \tau_{ik}^{T}\frac{\partial \tilde{u}_j}{\partial x_k} + \tau_{jk}^{T}\frac{\partial \tilde{u}_i}{\partial x_k} \tag{11}$$

$$\mathcal{D}_{ij} = \frac{\partial}{\partial x_k}\left[\left(\mu_{L} + \frac{\mu_{T}}{\sigma_k}\right)\frac{\partial}{\partial x_k}\left(\frac{-\tau_{ij}^{T}}{\bar{\rho}}\right)\right] \tag{12}$$

$$\begin{aligned}\Pi_{ij} = &-\left(C_1^0 + C_1^1\frac{\mathcal{P}}{\bar{\rho}\epsilon}\right)\bar{\rho}\epsilon b_{ij} + C_2\bar{\rho}k\widetilde{S}_{ij}^{D} \\ &+ C_3\bar{\rho}k\left[b_{ik}\widetilde{S}_{kj} + \widetilde{S}_{ik}b_{kj} - \frac{2}{3}b_{mn}\widetilde{S}_{mn}\delta_{ij}\right] - C_4\bar{\rho}k\left[b_{ik}\widetilde{R}_{kj} - \widetilde{R}_{ik}b_{kj}\right]\end{aligned} \tag{13}$$

Here, $\mathcal{P} = \mathcal{P}_{ij}\delta_{ij}/2$, $b_{ij} = \left(-\tau_{ij}^{T} - 2\bar{\rho}k\delta_{ij}/3\right)/2\bar{\rho}k$, $k = -\tau_{ij}^{T}\delta_{ij}/2\bar{\rho}$, μ_{T} is given by Eq. (29), and ϵ is obtained from a transport equation such as Eq. (27). The C_1^0, C_1^1, C_2, C_3, and C_4 scalar coefficients of the pressure strain model are assigned constant values as is the diffusion coefficient σ_k.

Algebraic Reynolds stress models make two assumptions to reduce the differential Reynolds stress transport equations into an algebraic form. One is a weak equilibrium assumption on the turbulence anisotropy, and the other is an assumption regarding the turbulent diffusion.[3,4]

$$\frac{Db_{ij}}{Dt} \approx 0 \tag{14}$$

$$\mathcal{D}_{ij} - \frac{\overline{\rho u_i'' u_j''}}{\bar{\rho}k}\mathcal{D} \approx \left(-2\mathcal{D}b_{ij}\right)\gamma_2 \qquad \gamma_2 = 0 \text{ or } 1 \tag{15}$$

where $\mathcal{D}$ is the diffusion of turbulent kinetic energy. In this work, $\gamma_2 = 1$ is assumed. The turbulent stress tensor is then expressed using a tensor basis representation composed of functions of the mean strain and rotation rate tensors.

$$\tau_{ij}^{T} = -\frac{2}{3}\bar{\rho}k\delta_{ij} - 2\bar{\rho}k\Bigg[G_1\frac{k}{\epsilon}\widetilde{S}_{ij}^{D} + G_2\left(\frac{k}{\epsilon}\right)^2\left(\widetilde{S}_{ik}^{D}\widetilde{R}_{kj} - \widetilde{R}_{ik}\widetilde{S}_{kj}^{D}\right) + G_3\left(\frac{k}{\epsilon}\right)^2\left(\widetilde{S}_{ik}^{D}\widetilde{S}_{kj}^{D} - \frac{1}{3}\widetilde{S}_{kl}^{D}\widetilde{S}_{kl}^{D}\delta_{ij}\right)\Bigg] \tag{16}$$

Substituting Eqs. (14–16) into the differential Reynolds stress transport equation and projecting onto the basis tensors forms a system of scalar equations for the G_1, G_2, G_3 tensor basis coefficients,

$$G_1^3 + G_1^2\left[\frac{-2L_1^0}{L_1^1\eta_1}\right] + G_1\left[\frac{\left(L_1^0\right)^2 + L_1^1L_2\eta_1 - \frac{2}{3}L_3^2\eta_1 - 2L_4^2\eta_2}{\left(L_1^1\eta_1\right)^2}\right] + \left[\frac{-L_1^0L_2}{\left(L_1^1\eta_1\right)^2}\right] = 0 \tag{17}$$

$$G_2 = \frac{-L_4G_1}{L_1^0 - L_1^1\left(G_1\eta_1\right)} \tag{18}$$

$$G_3 = \frac{2L_3G_1}{L_1^0 - L_1^1\left(G_1\eta_1\right)} \tag{19}$$

where the scalar L-terms are loosely used to group contributions from the corresponding C-coefficients of the pressure strain and compact the notation.

$$L_1^0 = \left(\frac{C_1^0}{2} - 1\right) + \gamma_2\left(\frac{\mathcal{P}}{\bar{\rho}\epsilon}\right)_\infty + \left(\frac{1-\phi}{2}\right)\left(C_1^1 + 2 - 2\gamma_2\right)\left(\frac{\mathcal{P}}{\bar{\rho}\epsilon}\right)_0 \tag{20}$$

$$L_1^1 = \left(C_1^1 + 2 - 2\gamma_2\right)\phi \tag{21}$$

$$L_2 = \left(\frac{C_2}{2} - \frac{2}{3}\right) \tag{22}$$

$$L_3 = \left(\frac{C_3}{2} - 1\right) \tag{23}$$

$$L_4 = \left(\frac{C_4}{2} - 1\right) \tag{24}$$

Algebraic stress models are used in conjunction with an underlying two-equation model, Eqs. (26–27), with $C_\mu = -G_1$ and the turbulent production $\mathcal{P}$ computed using the stress from Eq. (16). The quantity $(\mathcal{P}/\bar{\rho}\epsilon)_\infty$ is the equilibrium value of the ratio of production to dissipation, usually computed as $(C_{\epsilon 2} - 1)/(C_{\epsilon 1} - 1)$. For $\phi = 0$, a fixed value for the ratio of production to dissipation, denoted by $(\mathcal{P}/\bar{\rho}\epsilon)_0$, is used with a value often equal to the equilibrium value. For $\phi = 1$, that ratio is treated implicitly as part of the solution for τ_{ij}^T, since $\mathcal{P} \sim \tau_{ij}^T\widetilde{S}_{ji}$. That implicit treatment is what drives the nonlinearity in Eq. (17). Jongen and Gatski[5] have shown that the correct root to use from the G_1 cubic polynomial is the one with the lowest real part. In this work, we use $\phi = 1$ for a more self-consistent solution.

Eddy viscosity models, such as the popular series of k-ϵ models, use the Boussinesq approximation,[6] which assumes the turbulent stress is linearly related to the mean rate of strain through a scalar turbulent viscosity.

$$\tau_{ij}^{T} = 2\mu_T\widetilde{S}_{ij}^{D} - \frac{2}{3}\,\bar{\rho}k\,\delta_{ij} \tag{25}$$

$$\frac{\partial\left(\bar{\rho}k\right)}{\partial t} + \frac{\partial\left(\bar{\rho}\widetilde{u}_jk\right)}{\partial x_j} = \frac{\partial}{\partial x_j}\left[\left(\mu_L + \frac{\mu_T}{\sigma_k}\right)\frac{\partial k}{\partial x_j}\right] + \mathcal{P} - \rho\epsilon + L_k \tag{26}$$

$$\frac{\partial\left(\bar{\rho}\epsilon\right)}{\partial t} + \frac{\partial\left(\bar{\rho}\widetilde{u}_j\epsilon\right)}{\partial x_j} = \frac{\partial}{\partial x_j}\left[\left(\mu_L + \frac{\mu_T}{\sigma_\epsilon}\right)\frac{\partial\epsilon}{\partial x_j}\right] + C_{\epsilon 1}f_1\frac{\epsilon}{k}\mathcal{P} - C_{\epsilon 2}f_2\frac{\rho\epsilon^{\,2}}{k} + L_\epsilon \tag{27}$$

$$\mathcal{P} = \tau_{ij}^{T}\frac{\partial\widetilde{u}_i}{\partial x_j} \tag{28}$$

$$\mu_T = C_\mu f_\mu \bar{\rho} k^2 / \epsilon \tag{29}$$

In these equations, f_μ, f_1, and f_2 represent near-wall damping functions and L_k and L_ϵ represent near-wall source terms. C_μ is the eddy viscosity coefficient and σ_ϵ is a diffusion coefficient.

In each class of model, approximations are made to mimic the mean effect of the actual physical processes, which result in closure coefficients that must be calibrated through comparison with known or expected behavior. Each model may use a different procedure, different sets of experimental data, or different metrics for "optimizing" the results. Most of the time, calibration is done using a series of fundamental flows that isolate specific terms. Unfortunately, the details of how a model has been calibrated are not always fully disclosed and only the final coefficient values are given. The following paragraphs provide a short summary of the types of flows used to calibrate the various closure coefficients. For additional detail, see references 7, 8.

The eddy viscosity coefficient C_μ is often calibrated under the assumption of thin shear flows where the production of turbulent kinetic energy is nearly in balance with the turbulent dissipation rate ($\mathcal{P} \approx \bar{\rho}\epsilon$) together with experimental data such as Townsend[9] which indicates that the ratio of shear stress to turbulent kinetic energy $|\tau^T_{xy}|/\bar{\rho}k$ for a wide range of flows has nearly the same value of 0.3. The $C_{\epsilon 2}$ coefficient multiplying the dissipation term in the ϵ-transport equation is determined by analyzing the decay of isotropic homogeneous turbulence. The $C_{\epsilon 1}$ coefficient multiplying the production term in the ϵ-transport equation is obtained by applying the model to homogeneous turbulent shear flow. The diffusion coefficient σ_ϵ that also appears in the ϵ-transport equation is calibrated by analyzing the log-layer region of the turbulent boundary layer, and the diffusion coefficient σ_k in the k-transport equation is typically set to 1.0.

Differential and algebraic stress models require the calibration of a number of coefficients in the model for the pressure-strain correlation tensor, Eq. (13). Speziale, Sarkar, and Gatski[10] calibrate the "slow" pressure-strain coefficient C_1^0 from the decay of anisotropic homogeneous turbulence. The remaining pressure-strain coefficients C_1^1, C_3, and C_4 are chosen to provide agreement with homogeneous shear flow and rotating shear flow, whereas C_2 is determined from rapid distortion theory for homogeneously strained turbulence that is initially isotropic.

The benefit of the calibration procedures just described is that by using simple benchmark flows, individual closure coefficients can be isolated and calibrated independently. The shortcoming of these methods is that it is assumed that these coefficients will retain the same values for all types of flows. However, for any given flow there may be a particular combination of coefficients which would provide a better match with experimental data. Such retuning of the model coefficients is often frowned upon as fitting the CFD to the data.

Bradshaw[11] provides the compelling argument that the coefficients used in any modeled term will only assume constant values in the unlikely event that term exactly correlates with the physical term being modeled. More plausibly these coefficients will be different for different flows, and may vary from point to point within the same flow. Bradshaw[11] suggests that these coefficients may be improved by making them empirical functions of the local flow parameters such as the ratio of production to dissipation or a normalized measure of the flow invariants. Some limited attempts at varying coefficients have been tried in zonal models such as Birch, et al.,[12] which used different coefficient values in different regions of jet flow, and in two-layer eddy viscosity[13] and differential Reynolds stress models,[14] which transition between two sets of constant coefficients for near-wall and free shear flow regions.

Accepting the fact that the *modeled* forms of the turbulence closure equations are inevitably flawed due to the inability to precisely model each and every term in these equations, such models should be viewed as approximating the actual physical processes at work. Models calibrated against fundamental isotropic or homogeneous flows may be expected to work reasonably well in other "like" flows, but as the flow fields become more complex and the flow conditions become more extreme the accuracy of such models should be expected to decrease. Improving model predictions under these circumstances involves either extending the physical models used or recalibrating the model coefficients against a known dataset which is closer to the desired conditions.

A good analogy is the Taylor series representation of some arbitrary function. If the function is well behaved within a given neighborhood, then a reasonable approximation may be obtained using the first few terms in the Taylor series. The coefficients in the series are obtained by calibrating about the expansion location. As one moves outside of that calibration neighborhood, and particularly if the function is not well behaved, the error in the approximation increases. To correct for this, one can either include additional terms from the Taylor series or recalibrate the existing coefficients for use within the new neighborhood.

It is interesting to note that many of the early papers (i.e., references 15–17) describing the development and calibration of turbulence models refer to the use of "computer optimization" in determining appropriate values for many of the turbulence model coefficients. In most cases this terminology is a misnomer as no formal optimization procedures have been used and the objectives of the "optimization" are not rigorously defined. A more accurate description of those efforts would be *we ran a number of cases and these are the values that seemed to provide the best overall agreement with the available data.* One of the difficulties with a subjective method like this is in the repeatability of the results. What "looks good" to one person may not be optimal in another person's eyes. This is particularly true when several cases with different geometries or flow conditions are used in performing the evaluation and each evaluator imparts subconscious bias to the relative weighting of the cases involved.

The process of manually adjusting the closure coefficients to achieve better agreement with calibration data can be quite tedious. Due to the non-linear nature of the model equations, adjustments to individual coefficients can affect multiple aspects of the solution, yielding improvement in some areas and degradation in others. Deciding whether the net effect of such a change is an improvement or not can become a non-trivial task. In addition, a particular feature of a flow field may be affected by the contributions from different coefficients. This coupling between the various terms suggests that one must conduct the calibration in the multidimensional space of the coefficient set rather than calibrate each coefficient individually.

Numerical optimization procedures can be useful tools in improving the quality and repeatability of the calibration process. By their very nature these procedures require one to *quantify* the optimization objective, including the relative weightings of multi-objective optimizations. This forces one to carefully consider what the important metrics of the calibration are and to clearly define those objectives mathematically such that someone else could obtain the same result. Since numerical optimization procedures are automated, they can be used to easily and efficiently search multidimensional spaces and can be run to a tighter tolerance than could be achieved manually.

III. Numerical Optimization

A. Calculus-Based Optimization Methods

Calculus-based algorithms can be used to determine the local optimum within some neighborhood of the original starting location. These methods use information regarding the local derivatives of the optimization function to march in the direction that will yield an improved functional value compared to that of the current state.

Because these methods are based on the local gradient information, they are at best only guaranteed to locate the local optimum. Efforts to locate the global optimum usually involve repeating the optimization procedure from different starting locations or embedding pseudo-random perturbations into the marching procedure. If the optimization function is sufficiently smooth and slowly varying, then optima obtained from each starting location will coincide and will identify the global optimum. However, if the optimization function is rapidly varying, multimodal, or noisy within the domain of interest, then this marching procedure may identify a number of local optima, one or none of which may in fact be the global optimum.

Calculus-based algorithms can be computationally expensive as they require the calculation of the objective function and its derivatives with respect to each of the parameters involved. These methods require that the optimization function be not only continuous, but differentiable as well. Unfortunately, there is no guarantee that the optimization function to be composed for evaluating the turbulence model coefficients will be continuous, yet alone differentiable, over a broad domain. The use of particular combinations of model coefficients may cause the flow solver to completely fail, thus leaving the optimization function at those conditions undefined. In this regard, other optimization algorithms may prove to be more robust.

B. The Nelder-Mead Simplex Algorithm

The modified simplex search method of Nelder and Mead[18] is a method for optimizing a function of several variables without requiring the calculation of function derivatives. The method works by operating on a simplex in the space of the independent variables. In two dimensions a triangle forms a simplex. In three dimensions a pyramid forms a simplex. In n dimensions, a simplex is a polyhedron composed of $n+1$ points, which form its vertices. The function is evaluated at each vertex and a new, improved simplex can then be created by reflecting any properly chosen vertex through the centroid of the remaining vertices.

Consider the optimization of a function of two variables $f(x, y)$. For this case, $n = 2$ and the simplex is simply a triangle. The initial vertices are specified as $P_i = (x_i, y_i)$ for $i = 1, 2, ..., n+1$ and the corresponding functional values are denoted as f_i. The vertices are then sorted according to their functional values. This is illustrated in triangle ABC of Figure 1 where A is the best and C is the worst. If the function varies smoothly, then as one progresses along the line from C to A the functional value should improve. Likewise, as one progresses from C to B the functional value should also improve. Therefore, it is feasible that an even better functional value may occur at points on the other side of line AB. To test this, the worst point C is reflected through the centroid of the remaining vertices P to yield the new point D. If this point is found to be an improvement, then the search is proceeding in the proper direction and a new, improved simplex can be formed from ABD. However, it is also possible that proceeding farther in this same direction will yield an even better result. Another test point $2D$ is created by reflecting C twice as far through the centroid P. The better of D and $2D$ is then used along with A and B to form the new simplex and the procedure is repeated.

If D does not yield an improved functional value, then two additional points are considered. These points are the midpoints of lines CP and PD, labeled as E and F respectively. Only the best of these two is retained. If it is better than C, then the new simplex is formed from this point, A, and B. Otherwise, the new simplex is formed by retaining A and shrinking the other sides of the simplex. The entire procedure is then repeated on the new simplex until the size of the simplex has shrunk to within some desired tolerance.

The Nelder-Mead algorithm generally requires two function evaluations per cycle which makes it reasonably efficient. However, an additional n evaluations are needed every time the simplex shrinks. This method has also been found to be reliable in optimizing noisy functions, in part because the rate of expansion or contraction of the simplex is not directly tied to the gradient of the function being evaluated.

C. Genetic Algorithms

Genetic Algorithms (GA),[19,20] sometimes referred to as Evolutionary Strategies (ES), are based upon observations regarding the evolution of species. This so-called "survival of the fittest" hypothesis suggests that the strongest or "fittest" individuals in each generation are more likely to produce offspring than are the weaker members. As this mating process occurs over many generations, genes from the stronger individuals combine and become more prevalent among the species while the genes from the weaker individuals fade away or die out.

From a mathematical perspective, the optimization problem to be solved is described in terms of a number of design parameters. In the current context these are the turbulence model coefficients that need to be calibrated. Each of these design parameters represents a gene of the individual, and the collection of genes represents the individual's chromosomes. These genes are generally stored using a binary encoding which allows for a finite number of discrete possibilities. The gene length is therefore based on the number of discrete possibilities allowed. For example, a gene length of N would allow for 2^N possibilities of a particular design parameter. Each of the individual 0's and 1's used to encode the gene is called an allele.

Given an initially random population, the genetic algorithm uses the following steps to create all subsequent generations: (1) Selection, (2) Crossover, and (3) Mutation.

Selection refers to the process by which individuals are chosen for mating. This process must be constructed in such a way that members who are more fit have a greater chance of producing offspring. Several techniques for doing this have been devised, two of which are discussed here.

In roulette wheel selection, the cumulative fitness of the population is computed by summing the fitness of each individual. Then the probability of each individual mating is found by dividing that individual's fitness by the cumulative fitness of the population. In this way the fitness of each individual determines how large a slot on the roulette wheel that person has. Random pairs of parents are then selected for mating by spinning the wheel. With this selection method the parents traditionally produce two offspring, each of which contain some of the alleles of both parents though neither offspring has any common alleles with its sibling. For example, parents with chromosomes "00000" and "11111" may produce offspring "00011" and "11100".

In tournament selection, two random pairs of individuals are chosen from the population and the stronger (most fit) of each pair is allowed to mate. Each mating produces a single offspring, which may contain a mix of the genes of its parents. This random mating procedure continues until enough offspring are produced to replace the current population. Tournament selection is generally considered an improved selection technique.[21,22] One reason for this is that tournament selection provides greater selection pressure,[23] which is

to say that it provides a greater opportunity for the fittest individuals to be selected.

Crossover refers to the physical process by which the chromosomes of the parents are combined to form the chromosomes of the offspring. In single-point crossover, the parents' chromosomes are aligned one over the other. Then a random crossover position between chromosomes is selected and the child receives the chromosomes to the left of the crossover from one parent and the chromosomes to the right from the other. The crossover location may lie at the beginning or end of the chromosome string, in which case the offspring would inherit the complete chromosome set of one parent and none from the other. In multi-point crossover, the chromosomes are crossed at multiple locations. Each chromosome segment of the offspring is then randomly selected from the parents. In uniform crossover, each allele is randomly selected from the parents. Uniform crossover therefore represents an extreme case of multi-point crossover. With uniform crossover, it is still possible that an offspring may inherit all of its chromosomes from a single parent. However, this event is much less likely to occur than it is with single- or multi-point crossover.

Carroll[21] found that uniform crossover tends to preserve diversity in the genetic pool, which makes the genetic algorithm more robust. With uniform crossover, he observed a faster approach towards the optimal solution for his problem of interest. He also found that with uniform crossover he was able to obtain the solution to a particular order-3 deceptive function which single-point crossover was not able to optimize.

In nature, an individual's chromosomes sometimes mutate from those inherited from its parents. Mutation acts to throw some randomness into the chromosomes, which helps to freshen the gene pool. Otherwise the species could evolve to a certain point and then remain stagnant.

Two widely used methods to model the mutation are jump mutation and creep mutation. Jump mutation refers to the situation where one or more of an individual's genes may mutate to a randomly selected value that lies within the allowable range for that particular parameter. Thus, the value for a particular gene could jump from one end of the range to the other. With creep mutation, genes may randomly increase or decrease by one incremental value. This introduces a small perturbation to the gene, rather than the radically different value imposed by jump mutation. Jump and creep mutation are not mutually exclusive concepts. In fact, the two are usually used in concert with one another. Carroll[21] suggests using equal probabilities of each mutation event occurring.

Elitism is a mechanism used to ensure that the genes of the fittest individual get passed intact to the next generation. After the mating procedure is complete, the new population is checked to see whether the fittest individual has been replicated in the new generation. If not, then a random member of the new generation is removed and replaced by the fittest member of the previous generation. This procedure guarantees that the fittest individual of each generation will be no worse than than that of the previous generation (i.e., there is no chance of the best member regressing over time).

The genetic algorithm used in this study is actually a micro-GA (or μGA). The μGA begins with a very small initial population (in this study 5 individuals were used) and then proceeds in typical GA fashion. Within a few generations (usually 4 or 5) the population evolves to the point where the genetic makeup of each of the individuals is nearly identical and the population is said to have reached convergence. At this point, the best individual is retained, while the rest of the population is replaced by an entirely new set of random individuals. The process is then repeated using this new population.

There are several arguments for using a μGA rather than a standard GA. One is that the smaller population size results in less computation per generation. μGAs have also been demonstrated to converge faster than a standard GA,[21,24] and in some cases reach the optimum of deceptive functions that the standard algorithm cannot.[21] This ability to move past local optima is attributed to the constant infusion of new genetic information as the micro-population is reborn. Since the μGA is infused with new genetic material every time the population is reborn, there is no need to impose mutation on the evolutionary process. This simplifies the genetic algorithm.

Genetic algorithms are not without their share of limitations. Though genetic algorithms avoid the need to compute derivative information from the fitness function (and the computational costs associated with numerically evaluating the derivatives in multidimensional space), they must still perform an evaluation of the fitness function for *each individual* at *every generation*. With a typical genetic algorithm, hundreds (sometimes thousands) of individuals are needed to ensure enough diversity among the population for the algorithm to converge upon the true optimum. Therefore the time needed to perform these fitness evaluations quickly accumulates.

Another difficulty in using genetic algorithms is in determining when an optimum has been reached. Since a GA quasi-randomly searches the domain space without the use of gradient information, it contains

no mechanism for determining whether it has obtained an optimum value. At best it only knows that the current best value is no worse than that of the previous generation. As that best value improves, it generally takes a greater number of generations to find the next incremental improvement. In practice, the value is usually declared an optimum if it has remained unchanged over a certain number of generations.

IV. Numerical Method

For this work, the self-similar mixing layer code of Wilcox[7] was used. It solves the thin shear layer form of the compressible Navier-Stokes and turbulence model equations after applying three transformations. The first is a self-similar transformation that reduces the partial differential equations written in terms of (x, y) into ordinary differential equations written in terms of $\eta \sim y/x$. The second is a compressible flow transformation involving the density that reduces the equations to a form analogous to the incompressible equations. Lastly, the Rubel-Melnik[25,26] transformation is applied to improve numerical accuracy near the edges of the shear layer by mapping the finite edge location to infinity. The transformations and resulting equations are described in detail in Yoder.[27]

Non-uniform finite differencing is used to provide second-order expressions for the first and second derivatives and the equations are marched in pseudo-time to a steady state solution using the Crank-Nicolson[28] scheme. Solutions were deemed to be iteratively converged when the iterative error dropped below 10^{-7}, which represents a reduction of three to four orders of magnitude from the starting value. A few select cases were also run until the iterative error fell below 10^{-13}, but no significant differences between solutions were found. All calculations were performed using double precision (64 bit) arithmetic.

In order to assess the solution sensitivity to grid resolution, a grid refinement study was conducted for the conditions of the Delville[29] incompressible mixing layer. Shown in Figure 2 is the variation of the predicted mixing layer thickness with grid refinement. Here, the vorticity thickness $\delta_\omega = (\tilde{u}_1 - \tilde{u}_2)/(\partial\tilde{u}/\partial y)_{\max}$ is used as the measure of mixing layer thickness between the two streams, u_1 and u_2. These results were obtained using an algebraic stress model with standard k-ϵ coefficient values and the SSG[10] quasi-linear pressure-strain model. Similar results are obtained with other models. As is evident in this figure, results obtained using a minimum of 150 grid points are found to be within one percent of those obtained on the finest grid. This level of accuracy was considered sufficient for the present investigation.

Figure 3 compares the shear stress profiles obtained on these various computational grids. All of the results are in reasonably good agreement. However those obtained using less than 75 points clearly lack sufficient resolution to capture the shape of the peak region of the profile and also exhibit the largest differences near the edges of the shear layer. Wilcox[7] indicates that the mixing layer similarity code works best when at least 101 grid points are used. All of the results presented in section V have been obtained using a minimum of 201 grid points.

The self-similar mixing layer code was modified to be called as a subroutine from the optimization algorithms, passing in the closure coefficients and returning values from the flow simulation. The Nelder Mead Minimizer (NelderMeadMinimizer.f90) available from the National Institute of Standards and Technology (NIST) website was used to perform optimization using the simplex technique, starting with coefficient values of the baseline model. The Genetic Algorithm Driver of Carroll[21,30] was used to perform optimization using the genetic algorithm methodology. This software has the capability to run as either a traditional genetic algorithm or as a μGA. In the present investigation, the μGA option was used with a population of five, a random initial distribution, elitism to preserve the best member, tournament selection with one child per parents, uniform crossover with a probability of 0.5, and jump mutation with a probability of 0.02.

In order to numerically optimize the solution, one must provide an objective fitness function through which the solutions can be judged. For the planar mixing layer the fundamental parameter quantifying the mean flow solution is the mixing layer growth rate. Of course, the growth rate of the mixing layer is largely dependent upon the turbulent shear stress. Since the reduction in mixing layer growth rate in compressible flows appears to be related to changes in the turbulence anisotropy, it is also important to calibrate the Reynolds normal stresses for the baseline incompressible case. Therefore the goal of the optimization procedure was to find an acceptable compromise between matching the vorticity thickness growth rate and the similarity profiles of $-\overline{u'v'}$, $\overline{u'u'}$, $\overline{v'v'}$, and $\overline{w'w'}$ against the experimental data.

To quantify these figures of merit, a function was first defined which is a measure of the relative error

between a variable and a given data value.

$$error_{ABS}(var, value) = \min\left(1.0, \left|\frac{var}{value} - 1\right|\right) \tag{30}$$

This function varies from [0,1] with 0 being a perfect match and with the error capped at 1 (i.e., 100%). The fitness function is then computed using an equally weighted agglomeration of the above mentioned quantities of interest,

$$\begin{aligned} f_{ABS} = 1 - 0.2 * \Bigg\{ & \quad error_{ABS}\left(\frac{d\delta_w}{dx}\ ,\ 0.04995\right) \\ & + error_{ABS}\left(\frac{-\overline{u'v'}_{max}}{(U_1-U_2)^2}\ ,\ 0.01175\right) \\ & + error_{ABS}\left(\frac{\overline{u'u'}_{max}}{(U_1-U_2)^2}\ ,\ 0.02681\right) \\ & + error_{ABS}\left(\frac{\overline{v'v'}_{max}}{(U_1-U_2)^2}\ ,\ 0.01660\right) \\ & + error_{ABS}\left(\frac{\overline{w'w'}_{max}}{(U_1-U_2)^2}\ ,\ 0.02344\right)\Bigg\} \end{aligned} \tag{31}$$

with the numerical values obtained from the incompressible mixing layer experimental data of Delville.[29] This fitness function is also constructed to vary between [0,1] this time with 1 being a perfect score and 0 being the lower limit. An alternative fitness function, f_{SQR}, based on the square of the relative errors was also investigated.

$$error_{SQR}(var, value) = \min\left(1.0, \left[\frac{var}{value} - 1\right]^2\right) \tag{32}$$

For a single variable, optimizing the $error_{ABS}$ or $error_{SQR}$ will produce the same resultant coefficients although the level of fitness will differ. When multiple variables are agglomerated into the fitness function, the squared function will provide a larger weighting to variables that differ most from the target values.

Although getting the peak values of the turbulence profiles correct is an easily quantifiable objective, one would really like to obtain agreement with the entire similarity profile. To do this, an integral measure of the root mean square error was used.

$$error_{RMS}(var, data) = \min\left(1.0, \sqrt{\frac{\int\left[var_{(\eta)} - data_{(\eta)}\right]^2 d\eta}{\int d\eta}} \Bigg/ \max_{\eta}\ \left|data_{(\eta)}\right|\right) \tag{33}$$

$$\begin{aligned} f_{RMS} = 1 - 0.2 * \Bigg\{ & \quad error_{ABS}\left(\frac{d\delta_w}{dx}\ ,\ 0.04995\right) \\ & + error_{RMS}\left(\frac{-\overline{u'v'}}{(U_1-U_2)^2}\ ,\ \frac{-\overline{u'v'}_{data}}{(U_1-U_2)^2}\right) \\ & + error_{RMS}\left(\frac{\overline{u'u'}}{(U_1-U_2)^2}\ ,\ \frac{\overline{u'u'}_{data}}{(U_1-U_2)^2}\right) \\ & + error_{RMS}\left(\frac{\overline{v'v'}}{(U_1-U_2)^2}\ ,\ \frac{\overline{v'v'}_{data}}{(U_1-U_2)^2}\right) \\ & + error_{RMS}\left(\frac{\overline{w'w'}}{(U_1-U_2)^2}\ ,\ \frac{\overline{w'w'}_{data}}{(U_1-U_2)^2}\right)\Bigg\} \end{aligned} \tag{34}$$

Variation of some of the closure coefficients, in particular the diffusion coefficients, act to spread the similarity profile. This fitness function accounts for discrepancies at the edges of the shear layer which the others do not.

In order to facilitate the numerical integration, a Gaussian fit was used to represent the normalized stress profiles of the experimental data for the mixing layer case described in the next section. This curve is of the form

$$data_{(\eta)} = A \exp\left[\frac{-(\eta - \eta_0)^2}{2B^2}\right] \tag{35}$$

and the coefficients used to fit the various turbulence quantities are listed in Table 1. As shown in Figure 4, these curve fits and the standard error function velocity profile

$$U^* = \frac{\tilde{u} - \tilde{u}_2}{\tilde{u}_1 - \tilde{u}_2} = \frac{1}{2}\left[1 + \mathrm{erf}\,(\eta)\right] \tag{36}$$

provide a good representation of the experimental data for the present purpose.

In conducting any optimization procedure on the turbulence model, one must make certain that the parameters involved remain within physically acceptable limits. In the case of the genetic algorithm, the values of the coefficients are randomly selected from within a specified range. The range used in this study is listed in Table 2 and is centered about typical baseline values of the coefficients. The larger the search domain becomes, the more likely the odds that the genetic algorithm will select random values for the coefficients which cause the self-similar mixing layer code to diverge. This results in a fitness function of zero (the worst possible score) which adds nothing to the advancement of the optimum and merely increases the computational time necessary to perform the optimization.

Because the Nelder-Mead algorithm is a marching algorithm, the constraints must be embedded within the fitness function evaluation. The simplest method for achieving this is to force the fitness function to zero (again, the worst possible value) whenever one of the coefficients moves beyond the allowable range. For the present study, the turbulence model coefficients optimized with the Nelder-Mead algorithm were forced to remain positive. However, no upper limit on the allowable values was imposed. In this way, the Nelder-Mead optimization is allowed to search over a semi-infinite domain and therefore acts as a check against the more tightly constrained solution from the genetic algorithm.

V. Results

To demonstrate the feasibility of the optimization techniques, they were applied to obtain a better ASM calibration for the incompressible planar mixing layer case of Delville,[29] which has freestream velocities of 41.54 m/s and 22.40 m/s. The ASM formulation was chosen because it is the most economical model that can predict significant differences between the various normal stress components and would therefore be the most likely model to be used routinely for such problems. The Delville[29] data set was chosen because it is one of the most complete for this class of flow, with measurements of shear layer growth rate and detailed profiles of mean velocity and Reynolds stress components.

A. Baseline Assessment

Before applying the optimization procedures, a baseline assessment of different model types was performed. This included EVM, ASM, and RSM k-ϵ formulations using the "standard" high Reynolds number k-ϵ coefficients as well as those from Rumsey and Gatski.[31] These ASM and RSM formulations used the quasi-linear pressure-strain model of Speziale, Sarkar, and Gatski (SSG).[10] Also included in the baseline assessment were the Chien[32] k-ϵ eddy viscosity model and the ASM of Papp.[33] Table 3 summarizes all of the various model coefficients and Table 4 contains the model results.

Figure 5 compares the results from this baseline assessment. Included are similarity profiles of velocity, shear stress, turbulent kinetic energy, and the individual turbulent normal stresses. These results indicate a consistent trend between the eddy viscosity, algebraic stress, and Reynolds stress models when using a common set of coefficients. For example, the shear stress predicted by the k-ϵ model is noticeably larger than that predicted by the algebraic or differential Reynolds stress models. In addition, the differences between results using different coefficients for the same model type also display a consistent trend (i.e., the difference between k-ϵ results is comparable to the difference between ASM results). Overall, the use of the Rumsey-Gatski coefficients results in significantly less turbulence and lower mixing layer growth rates than

the standard coefficients. For these reasons, the standard coefficients appear to provide a better starting point for analyzing free shear flows and will serve as the baseline for the optimization studies.

It is also observed in Figure 5 that the Chien results are virtually identical to those of the standard k-ϵ model, which suggests that the difference between coefficients $C_{\epsilon 2} - C_{\epsilon 1}$ might be more of a driver for setting the turbulence levels than the actual values of $C_{\epsilon 1}$ or $C_{\epsilon 2}$. The Papp ASM results are important because they indicate that the difference in shear stress levels between k-ϵ and algebraic stress models can be eliminated through an adjustment of one of the pressure-strain coefficients used in the ASM. These cases provide valuable insight into how the coefficients may need to be adjusted to provide better predictions for free shear layer flows.

B. Model Coefficient Sensitivity Study

In order to assess which of the closure coefficients have the greatest influence on the mixing layer predictions, a coefficient sensitivity study was conducted by independently increasing the value of each closure coefficient by 10 percent over the ASM k-ϵ standard values. The predicted similarity profiles from this study are shown in Figure 6. According to these results, the two coefficients which most profoundly influence the turbulence levels are $C_{\epsilon 1}$ and $C_{\epsilon 2}$, which appear in the transport equation for the turbulent dissipation rate. Increasing $C_{\epsilon 1}$ effectively increases the production term in this transport equation. The resulting higher levels of turbulent dissipation inhibit the growth of turbulent kinetic energy and turbulent shear stress. Increasing the $C_{\epsilon 2}$ coefficient acts to increase the dissipation term in the ϵ-equation. This causes a reduction in the turbulent dissipation rate which allows for elevated turbulence levels.

Whereas the values of $C_{\epsilon 1}$ and $C_{\epsilon 2}$ appear to influence the predicted level of turbulence, it is the pressure-strain coefficients which determine how that turbulence is distributed between the normal stresses. From the sensitivity study shown in Figure 6, several trends can be found from variation of the pressure-strain coefficients. Overall, the various turbulence quantities are much less sensitive to changes in the pressure strain coefficients. The shear stress is most sensitive to C_2. An increase in this coefficient results in a small decrease in all of the predicted turbulence values. An increase in the C_1^0 or C_1^1 coefficients results in a very small transfer of turbulence energy from the streamwise to the transverse normal stress. An increase in C_3 results in a reduction in $\overline{u'u'}$ and $\overline{v'v'}$, and a slight increase in $\overline{w'w'}$. Increasing C_4 yields a small increase in $-\overline{u'v'}$ and $\overline{v'v'}$ with very little change in the other normal stresses.

C. Recalibration Study: C_2

For a thin shear flow such as the planar mixing layer, any deficiencies in predicting mean-flow properties such as the mixing layer growth rate are ultimately tied to deficiencies in predicting the turbulent shear stress. Therefore a primary goal of any recalibration should be to improve the shear-stress predictions. The standard values of the k-ϵ closure coefficients are well established, and the incompressible planar mixing layer results obtained using these coefficients with the Boussinesq expression for the Reynolds stresses have already been found to be satisfactory. It is only when the Boussinesq expression is replaced with that from the algebraic stress model that the turbulence levels are found to be underpredicted. This would seem to indicate that something within the algebraic stress model, rather than the k-ϵ equations, needs to be recalibrated. Therefore one should focus on making adjustments to the coefficients of the algebraic stress model (i.e., the pressure-strain coefficients) and only reluctantly set about modifying the values used in the k-ϵ equations.

Such was the approach taken by Papp et al.[33] who started with the standard k-ϵ model coefficients in conjunction with the quasi-linear pressure-strain model of Speziale-Sarkar-Gatski (SSG),[10] and found that by adjusting the C_2 pressure-strain coefficient one could achieve increased turbulence levels which were more representative of free shear flows. This adjustment of C_2 was found to only minimally impact the ASM predictions for fundamental turbulent flows.

Therefore, as part of the present investigation, a systematic variation of the C_2 coefficient was performed. The baseline ASM for this study used the standard high-Reynolds number k-ϵ model coefficients together with the SSG pressure-strain model. The results shown in Figure 7 confirm these findings. By reducing C_2 from the standard value of 0.36 to 0.25, the peak turbulent shear stress is brought into agreement with the Patel[34] data used for that previous calibration. In order to obtain agreement with the more complete shear stress data of Delville,[29] C_2 must be further reduced to 0.10.

The genetic algorithm was also used to numerically optimize C_2 using the fitness functions described in the previous section. These results, tabulated in Tables 3 and 4, suggest that C_2 should have a value in the range of 0.03 to 0.10, depending on which function is used for evaluation. Using the lower value for C_2 results in a slight overprediction of the peak shear stress, but the better agreement in the mixing layer growth rate and peak Reynolds normal stresses give it a better overall score. The Nelder-Mead algorithm was not applied to this case since it requires a minimum of two parameters.

D. Recalibration Study: C_2, C_3, C_4

The adjustment of C_2 affects the overall level of turbulence, but does not provide a mechanism for adjusting the individual Reynolds normal stresses. To achieve that effect requires modifying the other pressure-strain coefficients. Since the slow pressure-strain terms uniquely determine the model's ability to predict the decay of anisotropic turbulence, one would prefer not to modify the values of C_1^0 or C_1^1. Therefore, a study was undertaken to adjust the C_2, C_3, and C_4 coefficients and the results are shown in Figure 8.

The automated optimization approaches converge upon very similar profile solutions which agree well with that obtained by manually adjusting the coefficients. The largest discrepancy between these optimization results appears to be tied to a trade-off between matching the peaks in $\overline{u'u'}$ and $\overline{w'w'}$, with the Peak ABS function favoring $\overline{w'w'}$ and the RMS function favoring $\overline{u'u'}$. The Nelder-Mead method is more aggressive in this regard than the Genetic Algorithm. The Peak SQR results lie in the middle of these extremes, splitting the difference in the error of each term. In general, all of these results provide much better agreement with the experimental data for the normal stresses than those obtained by simply adjusting C_2. This is reflected in the improved fitness scores for this study, particularly the Peak ABS fitness metric.

It is interesting to note that during the manual optimization, a solution was found that required very little modification to the C_2 coefficient and thus it has been left at its standard value of 0.36. The numerical optimization results also indicate that C_2 remains near the standard value, in the range 0.34-0.44. However, in all cases the values for C_3 and C_4 are significantly higher than those in the baseline SSG model, [2.13-2.63, 1.09-1.32] vs [1.25, 0.40]. In addition, whereas the fitness scores from the two optimization methods are within 0.10% (Table 4), there are differences exceeding 10% between coefficient values (Table 3) when optimizing the Peak ABS error. This may be an indicator that the closure coefficients being optimized share influence over certain aspects of the solution, causing the fitness function to exhibit a number of local optima. Another possibility is that some coefficients only weakly affect the quantities of interest and so the fitness function is relatively flat within that dimension of the search space.

In order to investigate whether a local or global optimum was obtained, 4600 mixing layer simulations were computed for $C_2 \in [0.1, 0.8]$, $C_3 \in [0.1, 3.0]$, and $C_4 \in [0.1, 1.5]$ with a resolution of at least 0.1 for each coefficient. Three-dimensional visualization within this domain space determined that the fitness function is generally smooth and confirmed that a global optimum was indeed obtained by the Nelder-Mead method. To better understand how such different coefficient values resulted in similar fitness scores, an additional series of cases were computed for coefficient values that lie along the line between the Genetic Algorithm and Nelder-Mead sets. The coefficients along this line can be described by a one-dimensional parameterization

$$C(\xi) = C_{GA} + (C_{NM} - C_{GA})\,\xi \tag{37}$$

which interpolates between the Genetic Algorithm values ($\xi = 0$) and the Nelder-Mead values ($\xi = 1$). Values of ξ outside of this range extrapolate along the same line. Figure 9 shows the variation of each of the error terms as a function of the interpolation parameter. For the Peak ABS fitness objective, one can clearly see the competing errors between $\overline{u'u'}$, $\overline{w'w'}$, and to a much lessor extent the mixing layer growth rate. The GA has found a local optimum, whereas NM has found the global optimum. The fitness function in the intermediate region is nearly monotonic. Peak SQR and RMS fitness scores vary much less between optimization algorithms. For the Peak SQR case, the rate of change of errors in $\overline{u'u'}$ and $\overline{w'w'}$ virtually offset each other, resulting in a relatively constant average error. For the RMS case, each of the individual errors remains effectively constant.

E. Recalibration Study: All Pressure-Strain Coefficients

The question then arises as to whether the similarity results can be further improved by making adjustments to all of the pressure-strain coefficients. Therefore, in this study C_1^0 and C_1^1 are included in the recalibration of C_2, C_3, and C_4. Manual optimization of the coefficients was not attempted for this case

due to the complexity of the coefficient interactions. The results shown in Figure 10 are remarkably similar to the previous case. While the profiles obtained from the two optimization algorithms appear to be very consistent, there are again differences in the $\overline{u'u'}$ and $\overline{w'w'}$ normal stresses depending on the fitness function used. As before, the RMS function favors the former whereas the Peak ABS function favors the latter. The Nelder-Mead Peak ABS results accentuate this difference. Despite the additional degrees of freedom, these results do not appear to provide any significant improvement over those obtained by optimizing only C_2, C_3, and C_4. The tabulated values of the fitness functions (Table 4) also indicate little change, and in some instances the scores are fractionally worse than those obtained by optimizing only C_2, C_3, and C_4. Compared to the previous case, there is a general increase in C_1^0 and C_1^1 and a reduction in C_2 and C_4.

Figure 11 examines the variation of the fitness function along the parametric five-dimensional line that interpolates between the GA and NM solutions. Results for the Peak ABS optimization function again show there is a significant trade-off in the error of $\overline{u'u'}$ and $\overline{w'w'}$, with the GA identifying a local optimum and the NM method identifying an even better optimum. Differences between the GA and NM fitness values for the Peak SQR and RMS optimization functions are again much smaller than for the Peak ABS. For Peak SQR, there is a small trade-off in the error of $\overline{u'u'}$ and $\overline{w'w'}$, and the optimum appears to lie in between the GA and NM values. For the RMS fitness optimization, the individual errors are relatively constant, but fractional variations also lead to a optimum of the fitness function midway between the GA and NM values.

F. Recalibration Study: All k-ϵ and Pressure-Strain Coefficients

One can extend the recalibration effort to *all* of the closure coefficients (i.e., those associated with the k-ϵ transport equations in addition to the pressure-strain coefficients). In terms of the procedures used to calibrate the k-ϵ coefficients in the first place, such a recalibration cannot be rigorously justified unless used in conjunction with a model that switches between near-wall and free shear flow coefficient sets. In this study the intent is to see whether the ASM, given the utmost degree of flexibility in its coefficient values, yields any significant improvement over the previous optimization results.

The results of this study, shown in Figure 12, do indicate some improvement in the lateral extent of the turbulence profiles. This is due to modifications to the turbulent diffusion coefficients. However, it appears that cases which provide better agreement with the turbulence profiles on the high-speed side of the mixing layer ($\eta > 0$) tend to overpredict the turbulence levels on the low-speed side ($\eta < 0$). Near the edges of the mixing layer and particularly on the high-speed side, the experimental data indicates a much more gradual approach to the edge conditions. These findings suggest that the use of an enhanced diffusion model may be needed to provide better agreement with the data. However, such an improvement would likely work just as well for cases where fewer coefficients are recalibrated.

Figure 12 illustrates the danger that can occur when the fitness metric is too closely tied to a specific region of the flow. The Genetic Algorithm Peak ABS result provides excellent agreement with the target objective of matching the mixing layer peak turbulence values, but grossly overpredicts the turbulence at the edges of the shear layer because there is no constraint to prevent it from doing so. Interestingly, the Nelder-Mead method provides a solution with nearly identical peak turbulent values without as much lateral spread across the mixing layer.

Results of the parametric variation of coefficients between the GA and NM sets are shown in Figure 13. The fitness function is observed to be smooth and does not exhibit multiple inflection points within the intermediate region. The Nelder-Mead method provides the best optimum for each of the fitness functions. However, for the Peak ABS case and especially for the RMS case, the Genetic Algorithm provides a compelling local optimum. With increasing numbers of parameters one might expect there to be greater probability that various combinations would produce similar results. In the RMS case, where the GA and NM fitness scores are within less than 0.05%, the variation among the majority of coefficient values is quite large.

VI. Discussion

A. Which Optimization Algorithm is Fastest?

Figure 14 examines the efficiency of the optimization algorithms by plotting the overall fitness versus the number of function evaluations. The first thing to note is that the number of evaluations needed to achieve an optimum increases as the number of coefficients involved is increased. This is intuitive, since the dimensionality of the search space increases with each additional parameter. The other thing to note is that

in nearly every case the genetic algorithm is found to be slower, particularly in achieving the last few percent improvement. Due to the quasi-random nature of the algorithm, additional iterations are incurred until the next "event" occurs that results in an improvement. One could improve upon the method by adjusting some of the algorithm inputs or by using the genetic algorithm until it reaches a plateau of a given duration and switching to another algorithm (such as Nelder-Mead) to locally refine that optimum.

For the cases examined, the algorithms required 100 or more evaluations to obtain an optimum. Such calculations for self-similar flows only take a few minutes total on a desktop computer, and simple two-dimensional benchmark flows might be obtained in a few hours or days. However, more complicated three-dimensional simulations could take several weeks to complete. These costs must be considered when considering optimization procedures. For example, for the C_2 optimization, a simple parametric study was far more cost-effective than using the genetic algorithm.

B. Which Optimization Algorithm is Best?

For the most part, the Nelder-Mead method and Genetic Algorithm converge upon similar mixing layer profiles and fitness scores. However, there are considerable differences in the coefficient values, which suggests that the chosen fitness functions might have multiple local optima. Since the fitness function is constructed as an equally weighted agglomeration of the five fitness metrics, it acts as a simple superposition of the error quantities. Depending on their alignment, one could easily envision cases where multiple peaks occur. Differences observed when combining the magnitude of the errors (Peak ABS) versus the squares of the errors (Peak SQR) highlight the sensitivity to how these objectives are combined.

In the cases examined, the Nelder-Mead method was found to be superior to the genetic algorithm in terms of locating the better coefficient set. Examination of the fitness function within the parameterized space between the GA and NM coefficient sets indicates that the fitness is well behaved and without numerous local optima. Plots of the individual error terms show how changes in the coefficients manifest in the individual target objectives and how the trade-off between those objectives affect the overall fitness score. This analysis provides greater insight into the behavior of the system and confidence in the optimization approach.

As the number of degrees of freedom increases, so does the likelihood of additional local optima. Because the Nelder-Mead method has some similarity to a gradient marching algorithm, it is less likely to step away from one local optimum to find the next. Conversely, the Genetic Algorithm pseudo-randomly samples within the search space. In this light, the two algorithms should therefore be viewed as complementary tools. Concern over local versus global optima with the Nelder-Mead method can to some extent be mitigated by using different starting values. Likewise, improvements in the accuracy and efficiency of the Genetic Algorithm can be improved by feeding the optimum solution into the Nelder-Mead method.

C. Which Optimization Function is Best?

For the mixing layer, error metrics based on the peak turbulence values of the similarity profiles proved sufficient for obtaining improvement across a majority of the profile. This occurred because the self-similar profile shapes of the baseline model were already fairly consistent with the expected behavior, and optimizing for the peak values effectively scaled the entire profile. Use of the integral root-mean-square error metric only resulted in a significant difference when the diffusion coefficients were included as parameters in the optimization, since changes in the diffusion coefficients allowed for larger turbulence values near the edges of the mixing layer. The RMS error metric took this into account, and the optimization procedure attempted to minimize the error across the entire profile. This resulted in some sacrifice of the peak turbulence values in order to provide better agreement near the outer edges. None of the predictions were able to match the smooth tapering of the turbulence profiles at the edges of the shear layer, suggesting that physical modeling improvements to the diffusion terms may be needed.

For general use, something akin to the integral RMS function that accounts for errors throughout the flow field appears to be the best choice. The RMS function in this study assumes the experimental data (or curve fit) is sufficiently smooth to perform an integrated error across the profile. A similar effect could be achieved with more sparse data by aggregating the errors at multiple isolated points, provided the locations of those points are representative of the entire flow field and do not inadvertently introduce a bias towards one particular region. Additional work may be needed to address whether an integral error based on the L1 or L2 norm is best.

D. Which Coefficient Set is Best?

While the focus of this discussion is on the *methodology* for performing turbulence model recalibration through optimization, it is also important to discuss the *result* of which combination of model coefficients provides the best improvement. Since, as noted above, the Nelder-Mead algorithm provided superior results and the RMS function would be most appropriate for general application, this discussion is limited to those results. Because Nelder-Mead could not be applied to the single coefficient C_2 optimization, the optimal $C_2 = 0.05$ results from the parametric study are included. They are nearly identical to those of the Genetic Algorithm optimum. Tables 5 and 6 provide a direct comparison of the best optimization results for the four coefficient studies investigated. These results, which are a subset of those in Tables 3 and 4, are plotted in Figure 15.

As was noted in the discussion of each of the coefficient studies and is demonstrated by the tabulated RMS fitness scores, including additional model coefficients improves the agreement with the target objective. This should be intuitive, as increasing the degrees of freedom is expected to provide a result that is, at worst, no worse than one with fewer degrees. Any extra degrees of freedom that are unimportant would ideally retain the same value as the baseline set. Practically, however, such non-influential parameters could assume any value since they would not affect the output.

Reducing the C_2 coefficient produces a uniform increase in each of the peak turbulent stresses, whereas adjusting C_2, C_3, C_4 permits a significant adjustment of the anisotropy among the turbulent normal stresses. Including C_1^0 and C_1^1 in the optimization process results in a much smaller incremental adjustment of the turbulent normal stresses, but very little improvement in the fitness metric. Because these parameters are only weakly influential for this case, there is little motivation to change them from their baseline values. Optimizing all of the k-ϵ and ASM coefficients enables greater diffusion of turbulence near the shear layer edges and improvement in the integral RMS score, but no additional benefit in the middle of the mixing layer. The additional diffusion is still insufficient to predict the gradual tapering of the turbulence profiles. This indicates that while diffusion is important for the outer part of the shear layer, the present model form for diffusion lacks the physics necessary to represent the true behavior and a simple adjustment of diffusion coefficients does not compensate for this. Taking all of these findings into consideration, we would therefore recommend using the Nelder-Mead RMS optimized values of C_2, C_3, C_4 for near-term mixing layer problems and exploring more advanced diffusion models for the future.

VII. Conclusion

In this paper, formal optimization procedures are applied to the re-calibration of an explicit algebraic Reynolds stress model for the self-similar region of the incompressible planar mixing layer. This is done using various combinations of turbulence model coefficients and evaluating an optimization fitness function based upon the error in mixing layer growth rate and the normal and shear components of the Reynolds stresses. These studies indicate that significantly better agreement with experimental data can be obtained for this class of problem by recalibrating the turbulence model. As more coefficients (i.e., degrees of freedom) are included in that process, the fitness scores improve. However, one quickly reaches a state of diminishing returns. Adjustment of the rapid pressure strain coefficients C_2, C_3, and C_4 was found to be most effective in simultaneously improving the mixing layer growth rate and turbulence anisotropy values. Care should be taken to examine the sensitivity of the fitness function result to the coefficient set, as coefficients that are not influential or only very weakly influential for a particular case could assume arbitrary values. Such values could be highly inappropriate for other cases and should perhaps be left unchanged.

For the coefficient optimizations examined, the Nelder-Mead method was found to obtain a better optimum and in fewer function evaluations compared to the Genetic Algorithm. Optimization functions based upon the peak turbulence values in the middle of the mixing layer proved largely successful, because most changes in model coefficients result in scaling of the profile magnitudes without significant lateral spreading. However, inclusion of diffusion coefficients into the optimization set highlights the necessity of using an optimization function that accounts for the integrated error across the entire domain. It is therefore recommended that an integral L1 or L2 fitness function be used for general applications.

Despite similar turbulence profiles and optimization scores, the optimized model coefficients returned by Nelder-Mead and the Genetic Algorithm were found to differ substantially. Analysis of the individual error terms and overall fitness function within the optimization space between the two identified optima shows how changes in the model coefficients affect the errors of the target metrics and how the trade-offs between those

errors affect the overall optimization fitness score. In all of the cases examined, the Nelder-Mead method provided the better of the two optima, and no additional optima were observed within the intermediate space.

The techniques described in this effort could readily be applied to calibration of the model for other self-similar flows, such as jets and boundary layers, and might provide insight into how the model coefficients should vary in different flow regimes. Additional work is needed to extend the technique to more general applications and/or calibration involving multiple datasets. Among the issues that will need to be addressed are: weighting and combining of fitness metrics across a range of disparate calibration cases and/or geometries; defining appropriate fitness metrics for use with a three-dimensional volume solution and sparse experimental data; and the increased computational cost associated with obtaining those three-dimensional solutions.

References

[1]Reynolds, O., "On the Extent and Action of the Heating Surface for Steam Boilers," *Manchester Literary and Philosophical Society*, Vol. 14, 1874, pp. 7–12.

[2]Launder, B., Reece, G., and Rodi, W., "Pregress in the Development of a Reynolds-Stress Turbulence Closure," *Journal of Fluid Mechanics*, Vol. 68, No. 3, 1975, pp. 537–566.

[3]Gatski, T. B. and Jongen, T., "Nonlinear Eddy Viscosity and Algebraic Stress Models for Solving Complex Turbulent Flows," *Progress in Aerospace Sciences*, Vol. 36, No. 8, 2000, pp. 655–682.

[4]Gatski, T. and Rumsey, C., "Linear and Non-Linear Eddy Viscosity Models," *Closure Stategies for Turbulent and Transitional Flows*, edited by B. Launder and N. Sandham, Cambridge University Press, New York, 2002, pp. 9–46.

[5]Jongen, T. and Gatski, T., "A Unified Analysis of Planar Homogeneous Turbulence Using Single-Point Closure Equations," *Journal of Fluid Mechanics*, Vol. 399, 1999, pp. 117–150.

[6]Boussinesq, J., "Théorie de l'Écoulement Tourbillant," *Mem. Présentés par Divers Savants Acad. Sci. Inst. Fr.*, Vol. 23, 1877, pp. 43–50.

[7]Wilcox, D. C., *Turbulence Modeling for CFD*, DCW Industries, 2nd ed., 1998.

[8]Pope, S. B., *Turbulent Flows*, Cambridge University Press, Cambrigde, UK, 2000.

[9]Townsend, A. A., *The Structure of Turbulent Shear Flow*, Cambridge University Press, Cambridge, England, 2nd ed., 1976.

[10]Speziale, C. G., Sarkar, S., and Gatski, T. B., "Modelling the Pressure-Strain Correlation of Turbulence: An Invarient Dynamical Systems Approach," *Journal of Fluid Mechanics*, Vol. 227, 1991, pp. 245–272.

[11]Bradshaw, P., "Turbulence Modeling with Application to Turbomachinery," *Progress in Aerospace Sciences*, Vol. 32, 1996, pp. 575–624.

[12]Birch, S. F., Lyubimov, D. A., Secundov, A. N., and Yakubovsky, K. Y., "Numerical Modeling Requirements for Coaxial and Chevron Nozzle Flows," AIAA Paper 2003–3287, May 2003.

[13]Menter, F. R., "Two-Equation Eddy-Viscosity Turbulence Models for Engineering Applications," *AIAA Journal*, Vol. 32, No. 8, Aug. 1994, pp. 1598–1605, Presented as AIAA Paper 93–2906.

[14]Eisfeld, B. and Brodersen, O., "Advanced Turbulence Modelling and Stress Analysis for the DLR-F6 Configuration," AIAA Paper 2005–4727, June 2005.

[15]Jones, W. and Launder, B., "The Calculation of Low-Reynolds-Number-Phenomena with a Two-Equation Model of Turbulence," *International Journal of Heat and Mass Transfer*, Vol. 16, 1973, pp. 1119–1130.

[16]Hanjalic, K. and Launder, B., "A Reynolds Stress Model of Turbulence and its Application to Thin Shear Flow," *Journal of Fluid Mechanics*, Vol. 52, April 1972, pp. 609–638.

[17]Hanjalic, K. and Launder, B., "Contribution Towards a Reynolds-Stress Closure for Low-Reynolds-Number Turbulence," *Journal of Fluid Mechanics*, Vol. 74, April 1976, pp. 593–610.

[18]Nelder, J. A. and Mead, R., "A Simplex Method for Function Minimization," *The Computer Journal*, Vol. 7, Jan. 1965, pp. 308–313.

[19]Holland, J. H., *Adaptation in Natural and Artificial Systems*, Cambridge: MIT Press, 1975, 1992.

[20]Goldberg, D. E., *Genetic Algorithms in Search, Optimization and Machine Learning*, Addison-Wesley, Reading, Massachusetts, 1989.

[21]Carroll, D. L., "Genetic Algorithms and Optimizing Chemical Oxygen-Iodine Lasers," *Developments in Theoretical and Applied Mechanics*, edited by H. Wilson, R. Batra, C. Bert, A. Davis, R. Schapery, D. Stewart, and F. Swinson, Vol. XVIII, School of Engineering, The University of Alabama, 1996, pp. 411–424.

[22]Goldberg, D. E. and Deb, K., "A Comparative Analysis of Selection Schemes Used in Genetic Algorithms," *Foundations of Genetic Algorithms*, edited by G. J. E. Rawlins, Morgan Kaufmann Publishers, San Mateo, CA, 1991, pp. 69–93.

[23]Bäck, T., "Selective pressure in evolutionary algorithms: A characterization of selection mechanisms," *Proceedings of the First IEEE Conference on Evolutionary Computation*, 1994, pp. 57–62.

[24]Krishnakumar, K. S., "Micro Genetic Algorithms for Stationary and Nonstationary Function Optimization," *Proceedings of the SPIE Intelligent Control and Adaptive Systems Conference*, Vol. 1196, Academic Press, Philadelphia, PA, 7–8 Nov 1989, pp. 289–296.

[25]Rubel, A. and Melnik, R. E., "Jet, Wake, and Wall Jet Solutions Using a $k-\epsilon$ Turbulence Model," AIAA Paper 84–1523, June 1984.

[26]Paullay, A. J., Rubel, A., Melnik, R. E., Rudman, S., and Siclari, M. J., "Similarity Solutions for Plane and Radial Jets Using a $k - \epsilon$ Turbulence Model," *Journal of Fluids Engineering*, Vol. 107, March 1985, pp. 79–85.

[27]Yoder, D. A., *Algebraic Reynolds Stress Modeling of Planar Mixing Layer Flows*, Ph.D. thesis, University of Cincinnati, 2005.

[28]Crank, J. and Nicolson, P., "A Practical Method for Numerical Evaluation of Solutions of Partial Differential Equations of the Heat-Conduction Type," *Proceedings of the Cambridge Philosophical Society*, Vol. 43, 1947, pp. 50–67.

[29]Delville, Joël, *La décomposition orthogonale aux valeurs propres et l'analyse de l'organisation tridimensionnelle des écoulements turbulents cisaillés libres*, Ph.D. thesis, Université de Poitiers, 1995, See also AGARD Advisory Report No. 345 (1998).

[30]Carroll, D. L., "Chemical Laser Modeling with Genetic Algorithms," *AIAA Journal*, Vol. 34, No. 2, Feb. 1996, pp. 338–346.

[31]Rumsey, C. and Gatski, T., "Recent Turbulence Model Advances Applied to Multielement Airfoil Computations," *Journal of Aircraft*, Vol. 38, No. 5, Sept. 2001, pp. 904–910, Presented as AIAA Paper 2000–4323.

[32]Chien, K.-Y., "Predictions of Channel and Boundary-Layer Flows with a Low Reynolds Number Turbulence Model," *AIAA Journal*, Vol. 20, No. 1, Jan. 1982, pp. 33–38.

[33]Papp, J., Kenzakowski, D., and Dash, S., "Calibration and Validation of EASM Turbulence Model Jet Flowfields," AIAA Paper 2002–0855, Jan. 2002.

[34]Patel, R. P., "An Experimental Study of a Plane Mixing Layer," *AIAA Journal*, Vol. 11, No. 1, Jan. 1973, pp. 67–71.

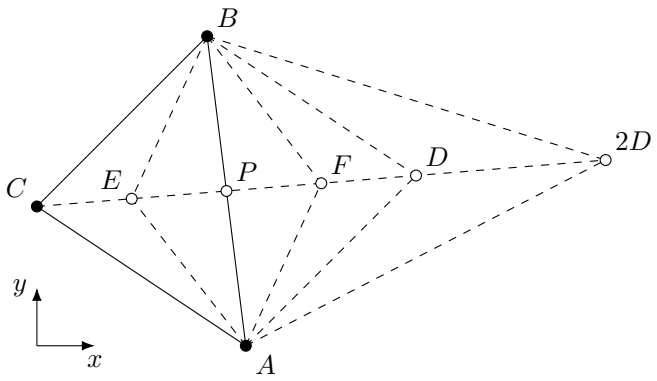

Figure 1: Notation used in the Nelder-Mead algorithm.

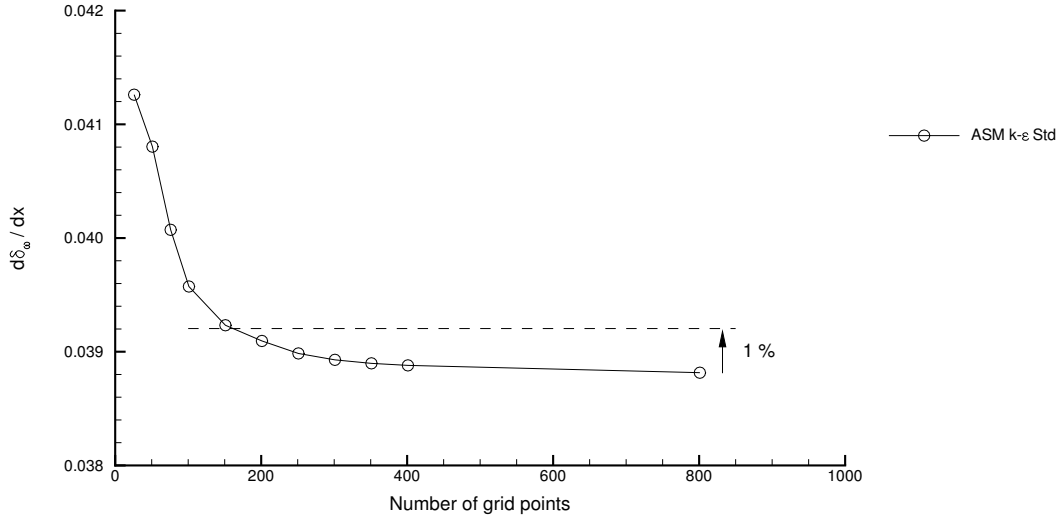

Figure 2: Effect of grid resolution on predicted mixing layer growth rate.

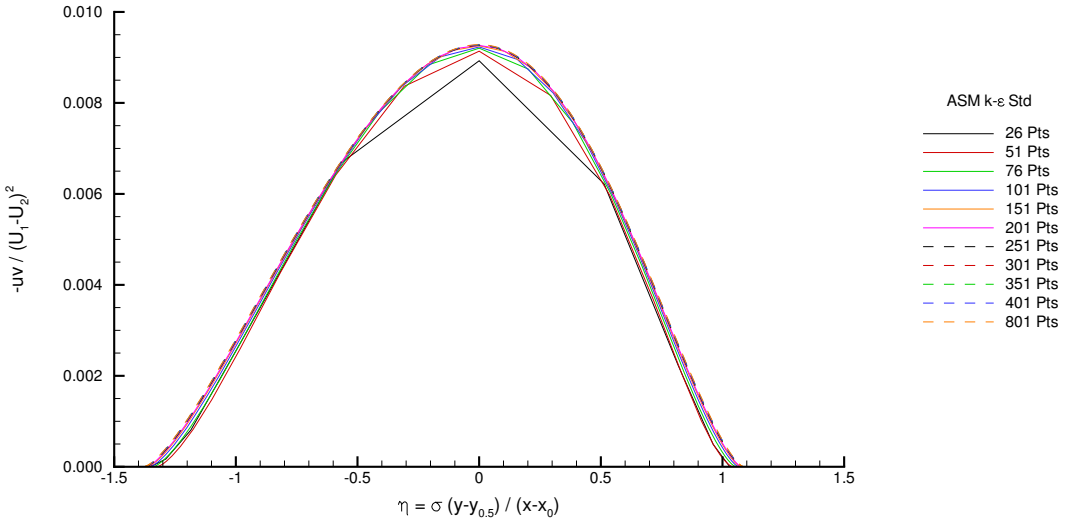

Figure 3: Effect of grid resolution on predicted shear stress profiles.

Quantity	A	B	η_0
$k/(U_1-U_2)^2$	0.033440	0.579847	0.043692
$\overline{u'u'}/(U_1-U_2)^2$	0.026840	0.577354	0.044200
$\overline{v'v'}/(U_1-U_2)^2$	0.016600	0.643587	0.038981
$\overline{w'w'}/(U_1-U_2)^2$	0.023440	0.537769	0.045144
$-\overline{u'v'}/(U_1-U_2)^2$	0.011750	0.560560	0.023762

Table 1: Gaussian curve-fit coefficients for Delville data.

Coeff.	Range	Coeff.	Range
C_μ	0.04 – 0.15	C_1^0	2.00 – 4.00
$C_{\epsilon 1}$	1.00 – 2.00	C_1^1	1.50 – 2.50
$C_{\epsilon 2}$	1.50 – 2.50	C_2	0.05 – 1.00
σ_k	0.10 – 1.20	C_3	0.50 – 3.00
σ_ϵ	0.50 – 2.00	C_4	0.10 – 1.50

Table 2: Range of Turbulence Model Coefficients Searched Using the Genetic Algorithm.

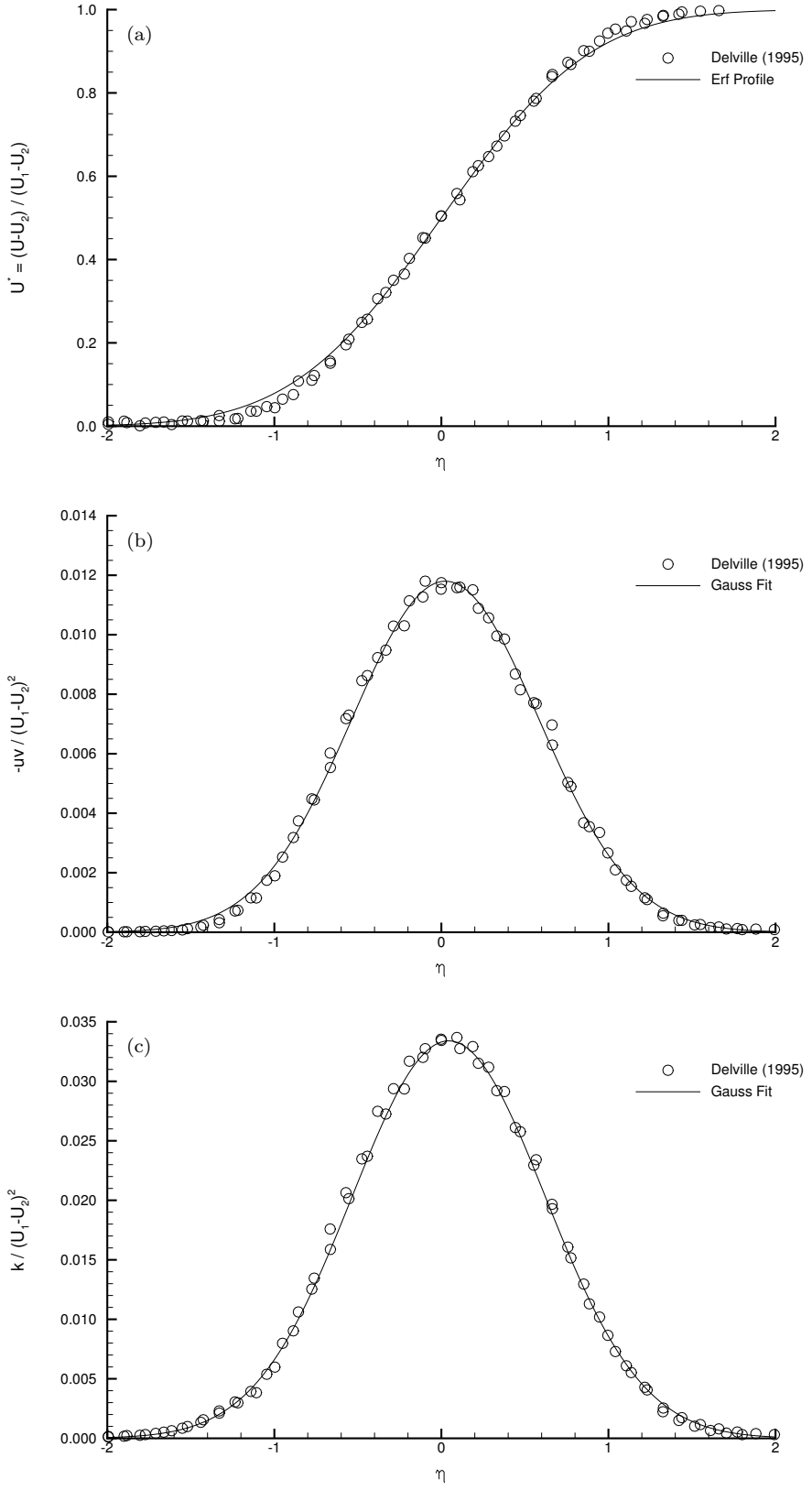

Figure 4: Gauss fit of incompressible mixing layer data.

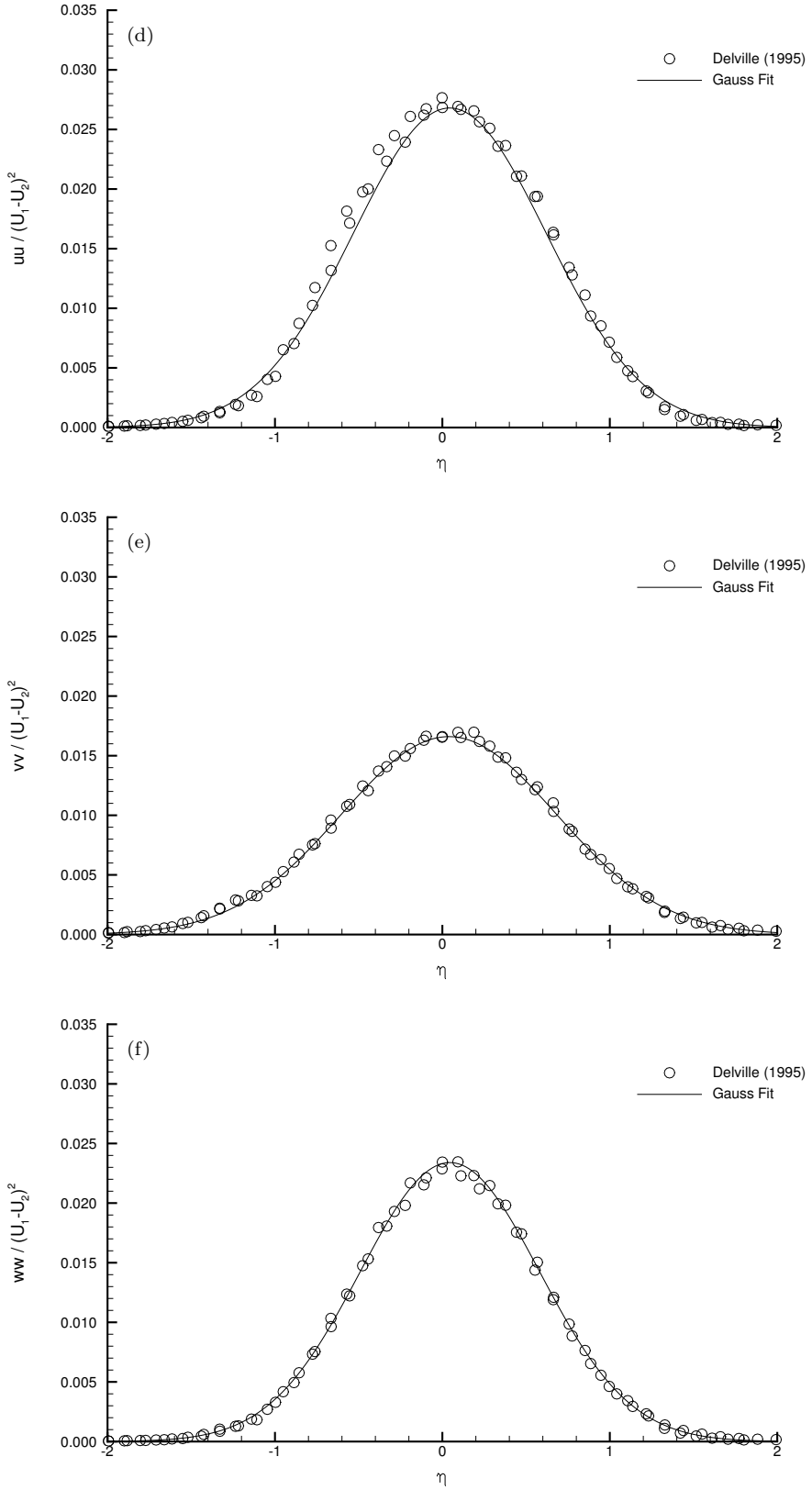

Figure 4: Gauss fit of incompressible mixing layer data. (Continued).

Model	C_μ	$C_{\epsilon 1}$	$C_{\epsilon 2}$	σ_k	σ_ϵ	C_1^0	C_1^1	C_2	C_3	C_4
Baseline Models										
k-ϵ Std	0.0900	1.4400	1.9200	1.0000	1.3000					
k-ϵ Chien	0.0900	1.3500	1.8000	1.0000	1.3000					
k-ϵ Rumsey-Gatski	0.0885	1.4400	1.8300	1.0000	1.4489					
ASM k-ϵ Std + SSG	0.0900	1.4400	1.9200	1.0000	1.3000	3.4000	1.8000	0.3600	1.2500	0.4000
ASM k-ϵ RG + SSG	0.0885	1.4400	1.8300	1.0000	1.4489	3.4000	1.8000	0.3600	1.2500	0.4000
ASM k-ϵ Papp + SSG*	0.0900	1.4300	1.9200	1.0000	1.3000	3.4000	1.8000	0.2500	1.2500	0.4000
RSM k-ϵ Std + SSG	0.0900	1.4400	1.9200	1.0000	1.3000	3.4000	1.8000	0.3600	1.2500	0.4000
RSM k-ϵ RG + SSG	0.0885	1.4400	1.8300	1.0000	1.4489	3.4000	1.8000	0.3600	1.2500	0.4000
Hand Optimization ASM k-ϵ										
HO C_2	0.0900	1.4400	1.9200	1.0000	1.3000	3.4000	1.8000	0.0100	1.2500	0.4000
	0.0900	1.4400	1.9200	1.0000	1.3000	3.4000	1.8000	0.0500	1.2500	0.4000
	0.0900	1.4400	1.9200	1.0000	1.3000	3.4000	1.8000	0.1000	1.2500	0.4000
	0.0900	1.4400	1.9200	1.0000	1.3000	3.4000	1.8000	0.1500	1.2500	0.4000
	0.0900	1.4400	1.9200	1.0000	1.3000	3.4000	1.8000	0.2000	1.2500	0.4000
	0.0900	1.4400	1.9200	1.0000	1.3000	3.4000	1.8000	0.2500	1.2500	0.4000
	0.0900	1.4400	1.9200	1.0000	1.3000	3.4000	1.8000	0.3000	1.2500	0.4000
	0.0900	1.4400	1.9200	1.0000	1.3000	3.4000	1.8000	0.3500	1.2500	0.4000
	0.0900	1.4400	1.9200	1.0000	1.3000	3.4000	1.8000	0.3600	1.2500	0.4000
HO C_2 C_3 C_4	0.0900	1.4400	1.9200	1.0000	1.3000	3.4000	1.8000	0.3600	2.3000	1.0500

Table 3: Turbulence model coefficients for baseline and optimized turbulence models.

Model	C_μ	$C_{\epsilon 1}$	$C_{\epsilon 2}$	σ_k	σ_ϵ	C_1^0	C_1^1	C_2	C_3	C_4
Genetic Algorithm Optimization ASM k-ϵ										
GA C_2 PeakABS	0.0900	1.4400	1.9200	1.0000	1.3000	3.4000	1.8000	0.1002	1.2500	0.4000
GA C_2 PeakSQR	0.0900	1.4400	1.9200	1.0000	1.3000	3.4000	1.8000	0.0328	1.2500	0.4000
GA C_2 RMS	0.0900	1.4400	1.9200	1.0000	1.3000	3.4000	1.8000	0.0503	1.2500	0.4000
GA C_2 C_3 C_4 PeakABS	0.0900	1.4400	1.9200	1.0000	1.3000	3.4000	1.8000	0.3803	2.1399	1.1575
GA C_2 C_3 C_4 PeakSQR	0.0900	1.4400	1.9200	1.0000	1.3000	3.4000	1.8000	0.3506	2.3751	1.1067
GA C_2 C_3 C_4 RMS	0.0900	1.4400	1.9200	1.0000	1.3000	3.4000	1.8000	0.4182	2.1395	1.1769
GA C_1^0 C_1^1 C_2 C_3 C_4 PeakABS	0.0900	1.4400	1.9200	1.0000	1.3000	3.0288	2.4392	0.3068	1.9856	1.0576
GA C_1^0 C_1^1 C_2 C_3 C_4 PeakSQR	0.0900	1.4400	1.9200	1.0000	1.3000	3.9499	1.9937	0.2459	2.3751	1.0063
GA C_1^0 C_1^1 C_2 C_3 C_4 RMS	0.0900	1.4400	1.9200	1.0000	1.3000	3.6877	2.4890	0.2112	2.1430	0.8812
GA All Coefs PeakABS	0.1347	1.2954	2.4053	0.5068	0.6170	3.3356	1.7859	0.5376	2.3090	1.1359
GA All Coefs PeakSQR	0.1342	1.3260	1.9192	0.8395	0.7962	3.5123	1.6150	0.5261	2.3028	1.1349
GA All Coefs RMS	0.1080	1.4014	1.9388	0.6949	0.8926	3.0159	2.1877	0.3409	2.0400	1.1083
Nelder-Mead Optimization ASM k-ϵ										
NM C_2 C_3 C_4 PeakABS	0.0900	1.4400	1.9200	1.0000	1.3000	3.4000	1.8000	0.4420	2.6322	1.3192
NM C_2 C_3 C_4 PeakSQR	0.0900	1.4400	1.9200	1.0000	1.3000	3.4000	1.8000	0.3425	2.3130	1.0912
NM C_2 C_3 C_4 RMS	0.0900	1.4400	1.9200	1.0000	1.3000	3.4000	1.8000	0.3984	2.1310	1.1179
NM C_1^0 C_1^1 C_2 C_3 C_4 PeakABS	0.0900	1.4400	1.9200	1.0000	1.3000	3.6968	2.8038	0.2630	2.7824	1.1889
NM C_1^0 C_1^1 C_2 C_3 C_4 PeakSQR	0.0900	1.4400	1.9200	1.0000	1.3000	4.6042	1.7834	0.1967	2.3570	0.9531
NM C_1^0 C_1^1 C_2 C_3 C_4 RMS	0.0900	1.4400	1.9200	1.0000	1.3000	3.7555	2.4154	0.2252	1.9895	0.9103
NM All Coefs PeakABS	0.1407	1.4321	2.1309	0.7654	0.7697	4.1236	2.5757	0.3843	2.3344	1.0050
NM All Coefs PeakSQR	0.1421	1.4513	2.1095	0.8822	0.9124	3.2188	2.9708	0.3869	2.3385	1.0035
NM All Coefs RMS	0.1754	1.4427	2.0117	3.6161	1.9771	0.4043	2.1671	1.1850	2.1671	1.1850

Table 3: Turbulence model coefficients for baseline and optimized turbulence models (Continued).

Case	$d\delta_\omega/dx$	Peak Values $-uv/\Delta U^2$	$uu/\Delta U^2$	$vv/\Delta U^2$	$ww/\Delta U^2$	$k/\Delta U^2$	Fitness Score Peak ABS	Peak SQR	RMS
Experiment									
Delville Data	0.04995	0.01175	0.02684	0.01660	0.02344	0.03368	1.00000	1.00000	1.00000
Baseline Models									
k-ϵ Std	0.04764	0.01070	0.02070	0.02070	0.02070	0.03106	0.85443	0.97258	0.93345
k-ϵ Chien	0.04768	0.01070	0.02070	0.02070	0.02070	0.03105	0.85454	0.97259	0.93364
k-ϵ Rumsey-Gatski	0.03860	0.00882	0.01764	0.01764	0.01764	0.02647	0.77412	0.94074	0.88954
ASM k-ϵ Std + SSG	0.03910	0.00926	0.02922	0.01298	0.01729	0.02975	0.80035	0.95674	0.89855
ASM k-ϵ RG + SSG	0.03349	0.00797	0.02514	0.01114	0.01486	0.02557	0.71803	0.90829	0.85890
ASM k-ϵ Papp + SSG	0.04526	0.01059	0.03046	0.01389	0.01829	0.03132	0.85787	0.97766	0.92687
RSM k-ϵ Std + SSG	0.04091	0.00949	0.03151	0.01163	0.01691	0.03002	0.77495	0.94653	0.89695
RSM k-ϵ RG + SSG	0.03493	0.00814	0.02689	0.01007	0.01454	0.02575	0.72334	0.90318	0.85905
Hand Optimization ASM k-ϵ									
HO C_2	0.04982	0.01247	0.03090	0.01446	0.01883	0.03209	0.89173	0.98358	0.94111
	0.04968	0.01216	0.03079	0.01435	0.01871	0.03192	0.89504	0.98360	0.94170
	0.04904	0.01175	0.03062	0.01419	0.01855	0.03168	0.89740	0.98306	0.94009
	0.04795	0.01132	0.03043	0.01401	0.01837	0.03141	0.88359	0.98164	0.93625
	0.04640	0.01087	0.03020	0.01381	0.01817	0.03109	0.86727	0.97899	0.93024
	0.04449	0.01040	0.02994	0.01359	0.01793	0.03073	0.84879	0.97468	0.92233
	0.04223	0.00990	0.02964	0.01333	0.01767	0.03032	0.82810	0.96820	0.91259
	0.03964	0.00937	0.02930	0.01304	0.01736	0.02985	0.80516	0.95896	0.90104
	0.03910	0.00926	0.02922	0.01298	0.01729	0.02975	0.80035	0.95674	0.89855
HO C_2 C_3 C_4	0.05043	0.01168	0.02555	0.01574	0.02219	0.03174	0.96622	0.99841	0.94993

Table 4: Incompressible mixing layer results for baseline and optimized turbulence models.

Case	$d\delta_\omega/dx$	Peak Values $-uv/\Delta U^2$	$uu/\Delta U^2$	$vv/\Delta U^2$	$ww/\Delta U^2$	$k/\Delta U^2$	Fitness Score Peak ABS	Peak SQR	RMS
Genetic Algorithm Optimization ASM k-ϵ									
GA C_2 PeakABS	0.04903	0.01175	0.03062	0.01419	0.01855	0.03168	0.89741	0.98305	0.94008
GA C_2 PeakSQR	0.04976	0.01230	0.03084	0.01440	0.01876	0.03200	0.89368	0.98363	0.94158
GA C_2 RMS	0.04968	0.01216	0.03079	0.01434	0.01871	0.03192	0.89506	0.98360	0.94170
GA C_2 C_3 C_4 PeakABS	0.05080	0.01174	0.02532	0.01660	0.02168	0.03180	0.97012	0.99817	0.94858
GA C_2 C_3 C_4 PeakSQR	0.05120	0.01192	0.02525	0.01601	0.02257	0.03192	0.96562	0.99860	0.94622
GA C_2 C_3 C_4 RMS	0.04995	0.01147	0.02508	0.01658	0.02155	0.03161	0.96572	0.99773	0.95243
GA C_1^0 C_1^1 C_2 C_3 C_4 PeakABS	0.05045	0.01175	0.02580	0.01660	0.02113	0.03176	0.97053	0.99774	0.95033
GA C_1^0 C_1^1 C_2 C_3 C_4 PeakSQR	0.05118	0.01193	0.02536	0.01602	0.02245	0.03192	0.96555	0.99862	0.94639
GA C_1^0 C_1^1 C_2 C_3 C_4 RMS	0.04995	0.01159	0.02592	0.01587	0.02154	0.03166	0.96542	0.99802	0.95244
GA All Coefs PeakABS	0.04989	0.01154	0.02679	0.01652	0.02347	0.03336	0.99462	0.99993	0.88819
GA All Coefs PeakSQR	0.05063	0.01159	0.02682	0.01661	0.02350	0.03346	0.99380	0.99993	0.95396
GA All Coefs RMS	0.04994	0.01182	0.02537	0.01609	0.02094	0.03120	0.96031	0.99692	0.96208
Nelder-Mead Optimization ASM k-ϵ									
NM C_2 C_3 C_4 PeakABS	0.05113	0.01175	0.02365	0.01660	0.02340	0.03183	0.97117	0.99707	0.94548
NM C_2 C_3 C_4 PeakSQR	0.05118	0.01193	0.02544	0.01604	0.02236	0.03192	0.96549	0.99863	0.94645
NM C_2 C_3 C_4 RMS	0.04995	0.01149	0.02541	0.01630	0.02153	0.03162	0.96501	0.99794	0.95245
NM C_1^0 C_1^1 C_2 C_3 C_4 PeakABS	0.05085	0.01175	0.02356	0.01658	0.02344	0.03179	0.97170	0.99695	0.94682
NM C_1^0 C_1^1 C_2 C_3 C_4 PeakSQR	0.05130	0.01192	0.02546	0.01603	0.02235	0.03192	0.96537	0.99862	0.94583
NM C_1^0 C_1^1 C_2 C_3 C_4 RMS	0.04995	0.01157	0.02602	0.01621	0.02107	0.03165	0.96593	0.99761	0.95244
NM All Coefs PeakABS	0.04995	0.01175	0.02684	0.01660	0.02344	0.03344	0.99998	1.00000	0.94864
NM All Coefs PeakSQR	0.05006	0.01172	0.02683	0.01661	0.02345	0.03345	0.99871	1.00000	0.95461
NM All Coefs RMS	0.04995	0.01145	0.02438	0.01583	0.02098	0.03059	0.94633	0.99556	0.96241

Table 4: Incompressible mixing layer results for baseline and optimized turbulence models (Continued).

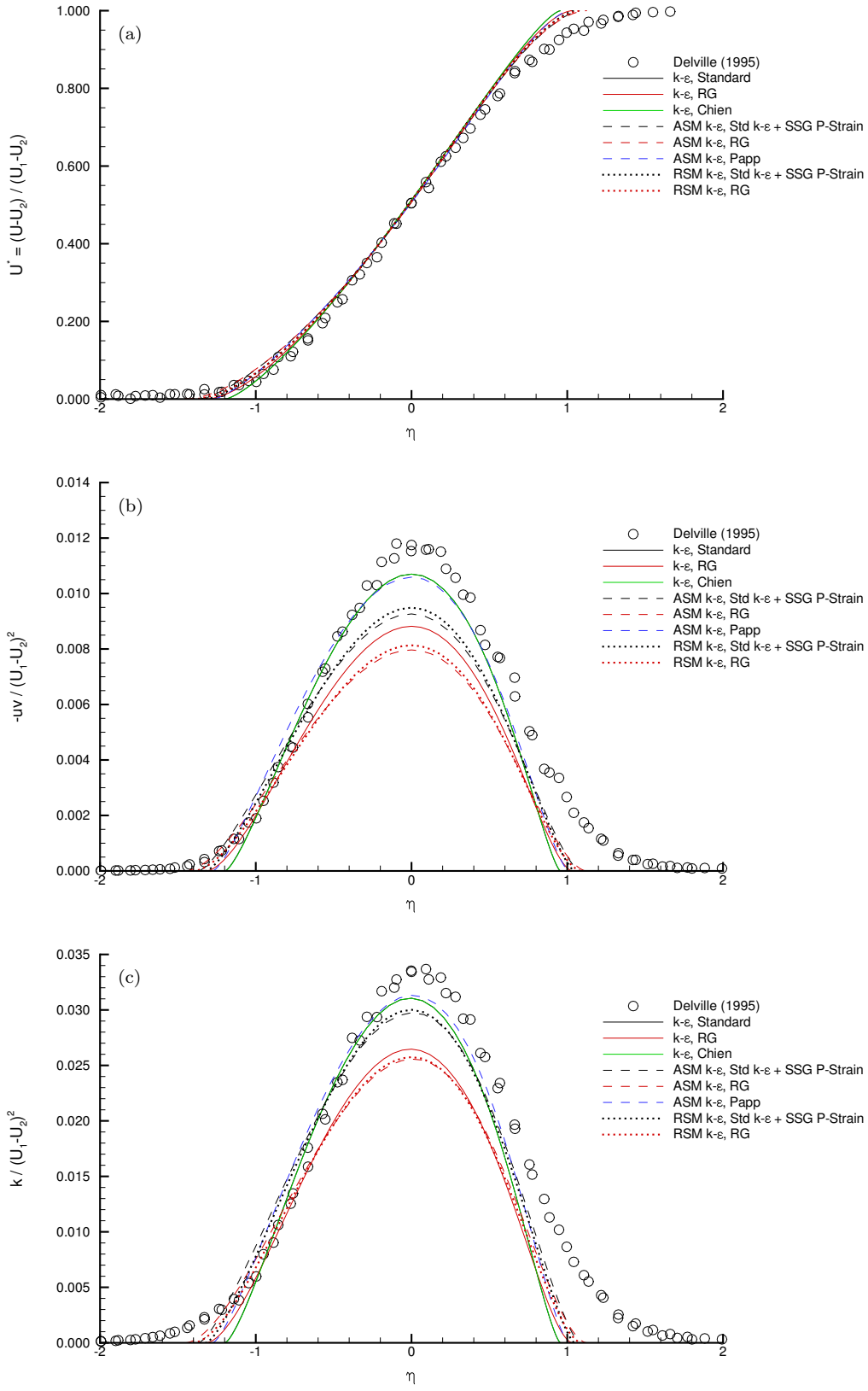

Figure 5: Predicted baseline similarity profiles of the incompressible mixing layer.

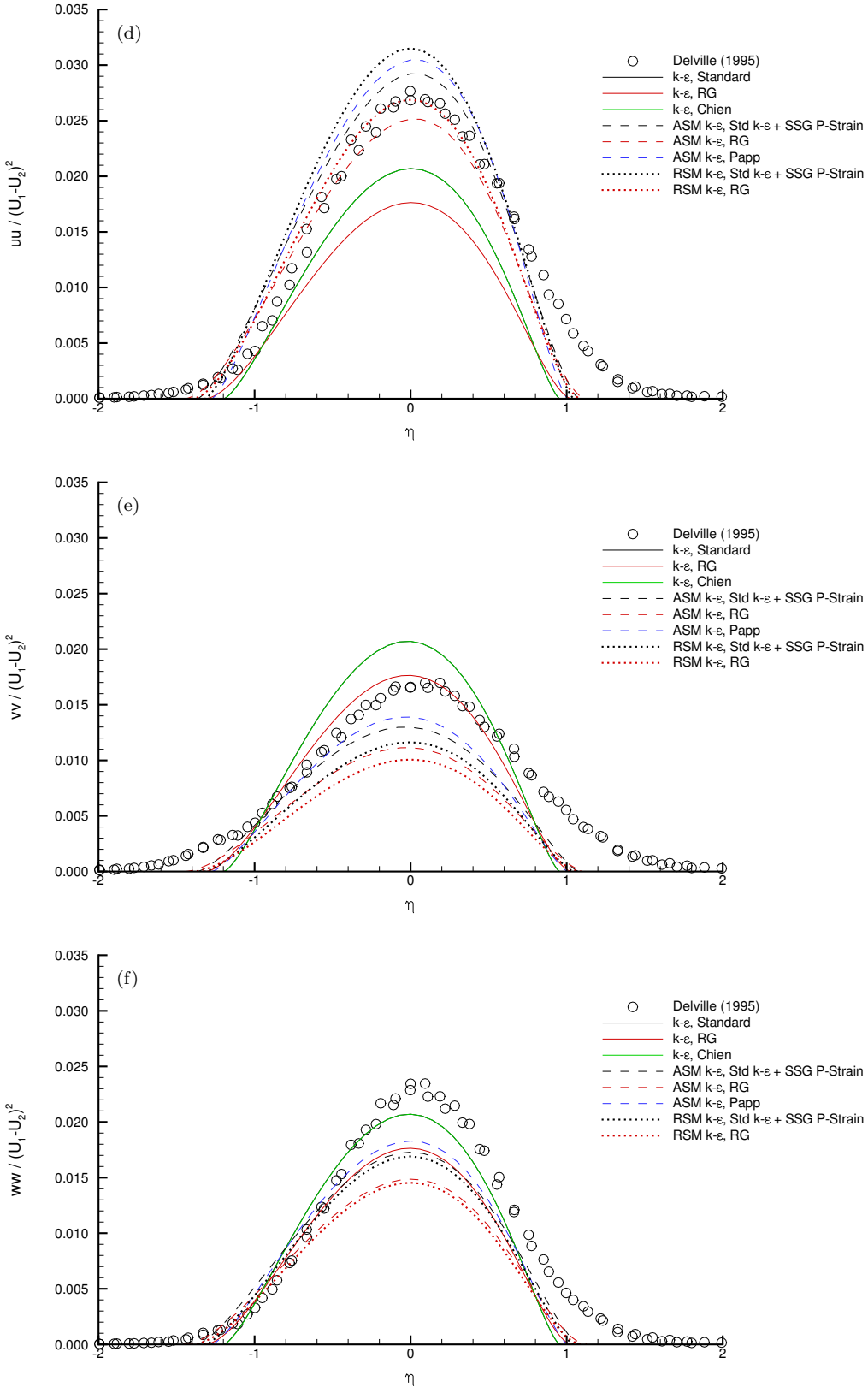

Figure 5: Predicted baseline similarity profiles of the incompressible mixing layer (Continued).

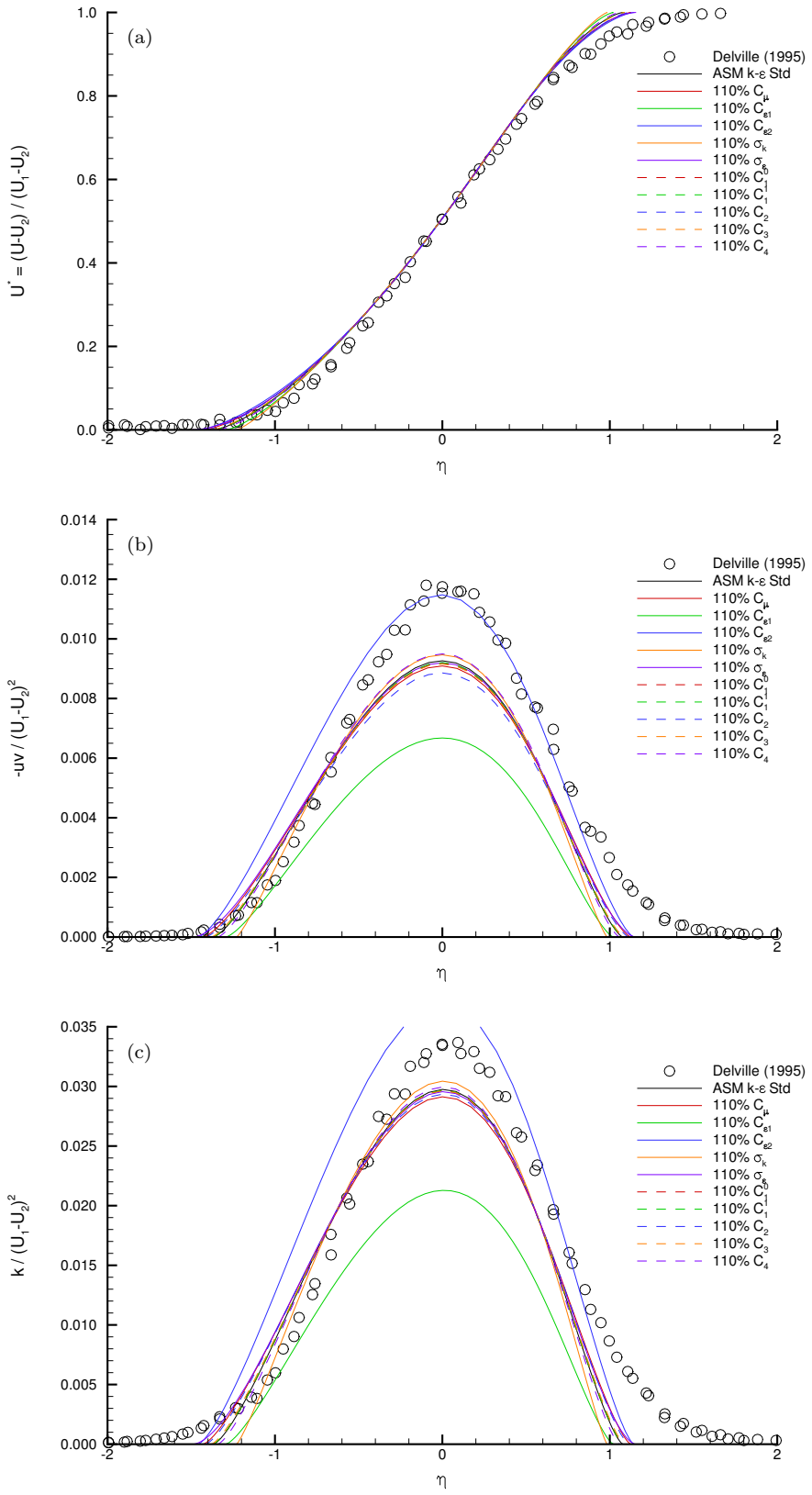

Figure 6: Effect of a 10% change in closure coefficients on predicted similarity profiles of the incompressible mixing layer.

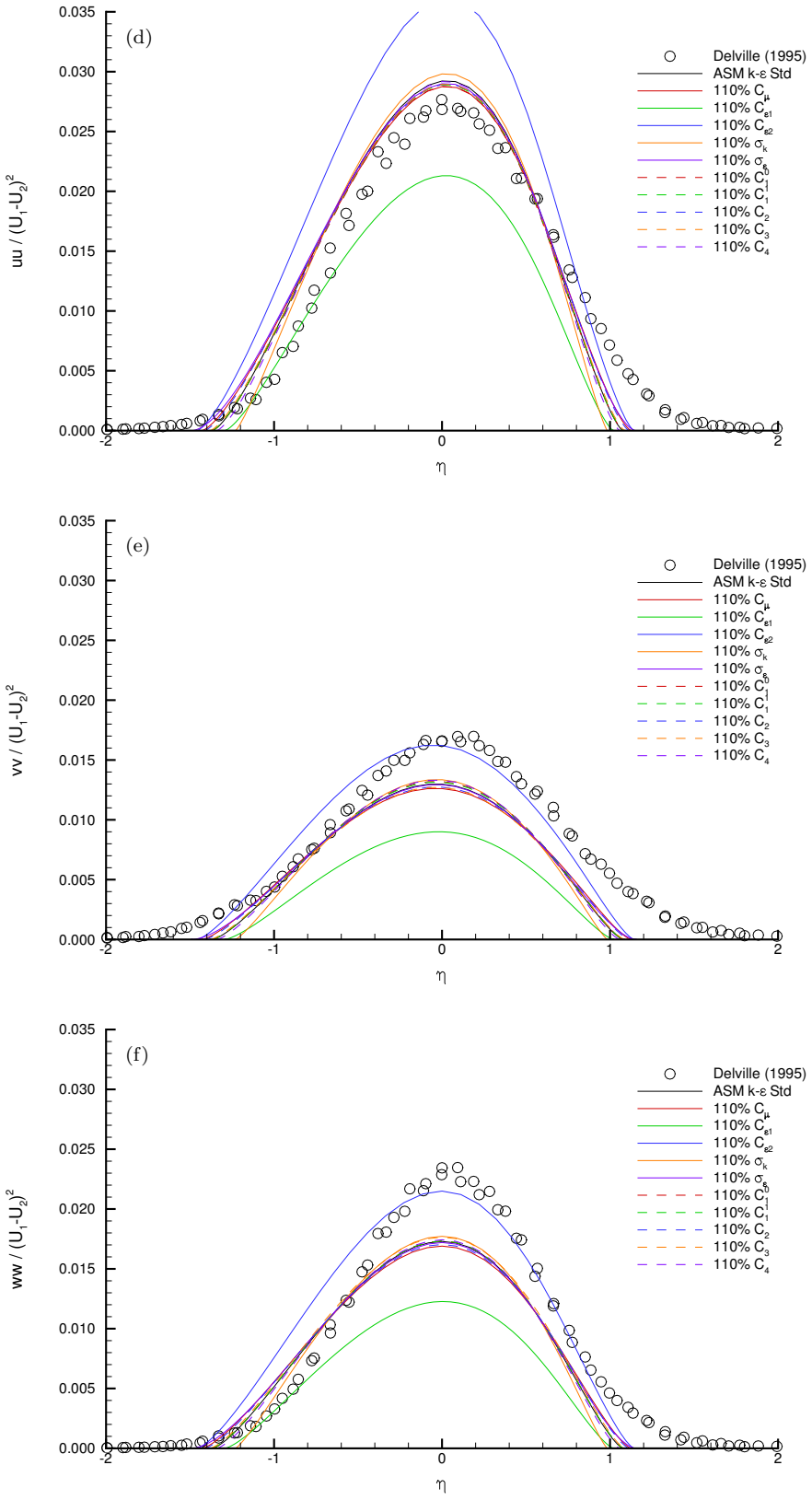

Figure 6: Effect of a 10% change in closure coefficients on predicted similarity profiles of the incompressible mixing layer (Continued).

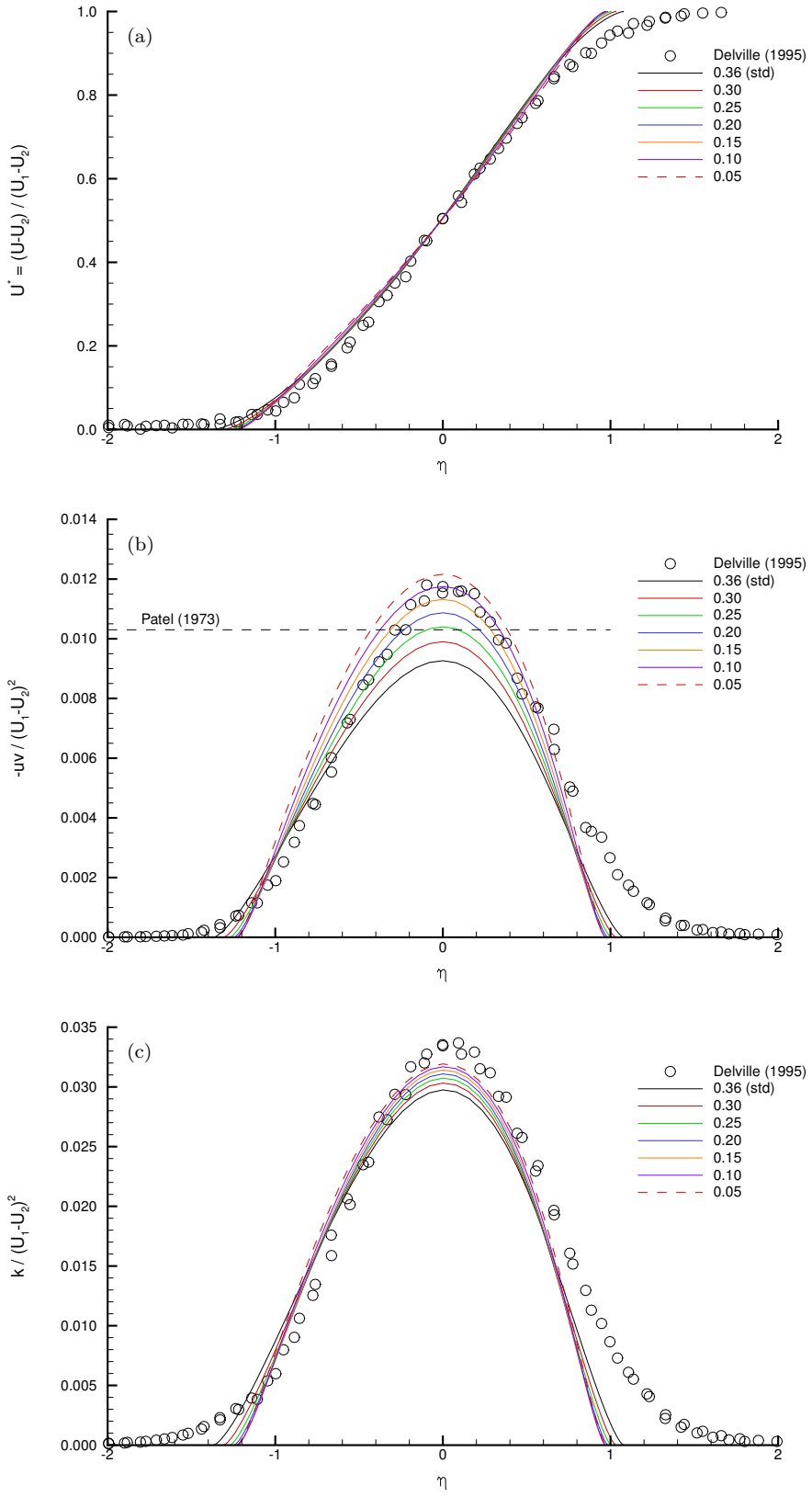

Figure 7: Recalibration study involving the C_2 coefficient.

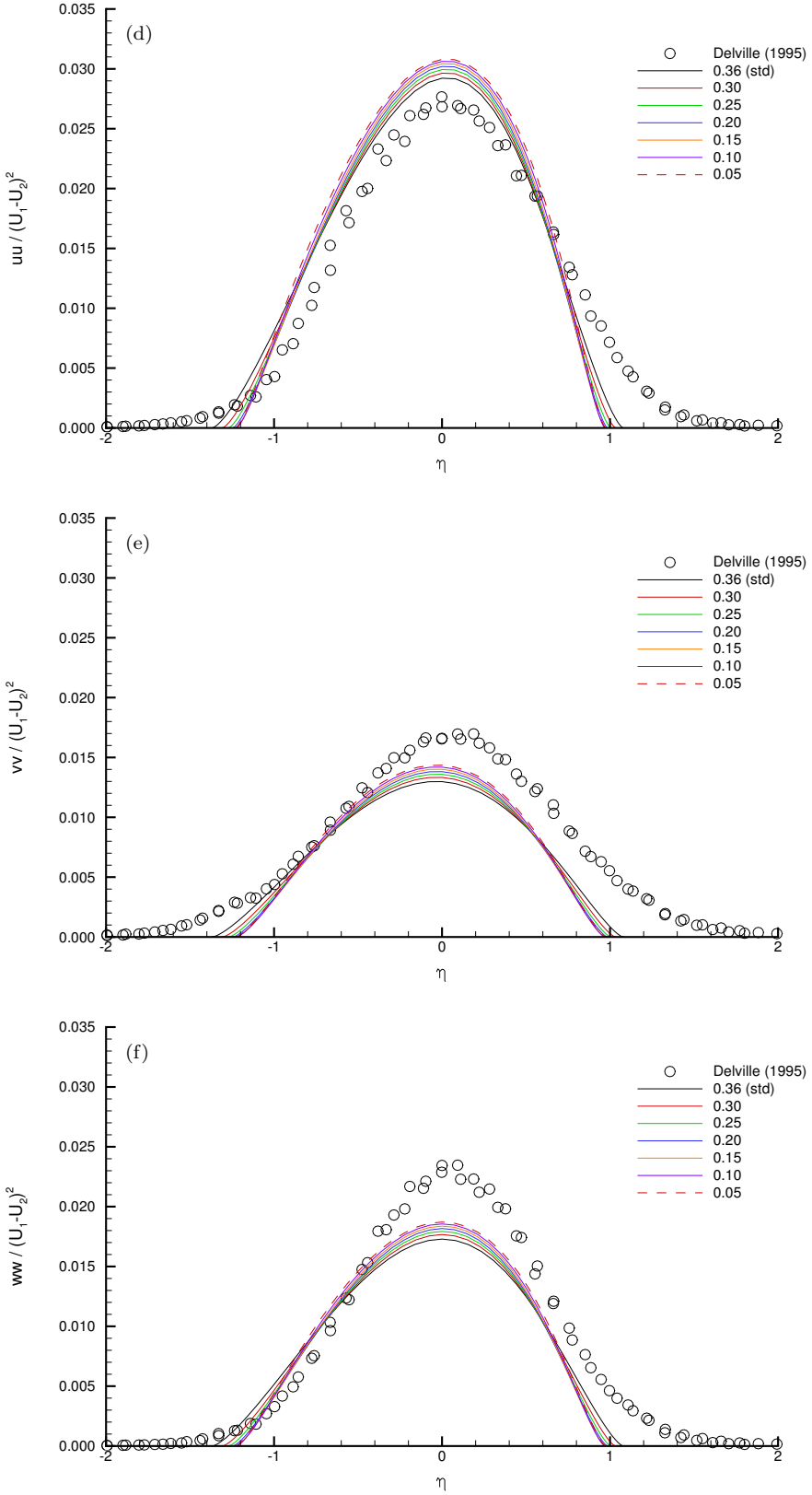

Figure 7: Recalibration study involving the C_2 coefficient (Continued).

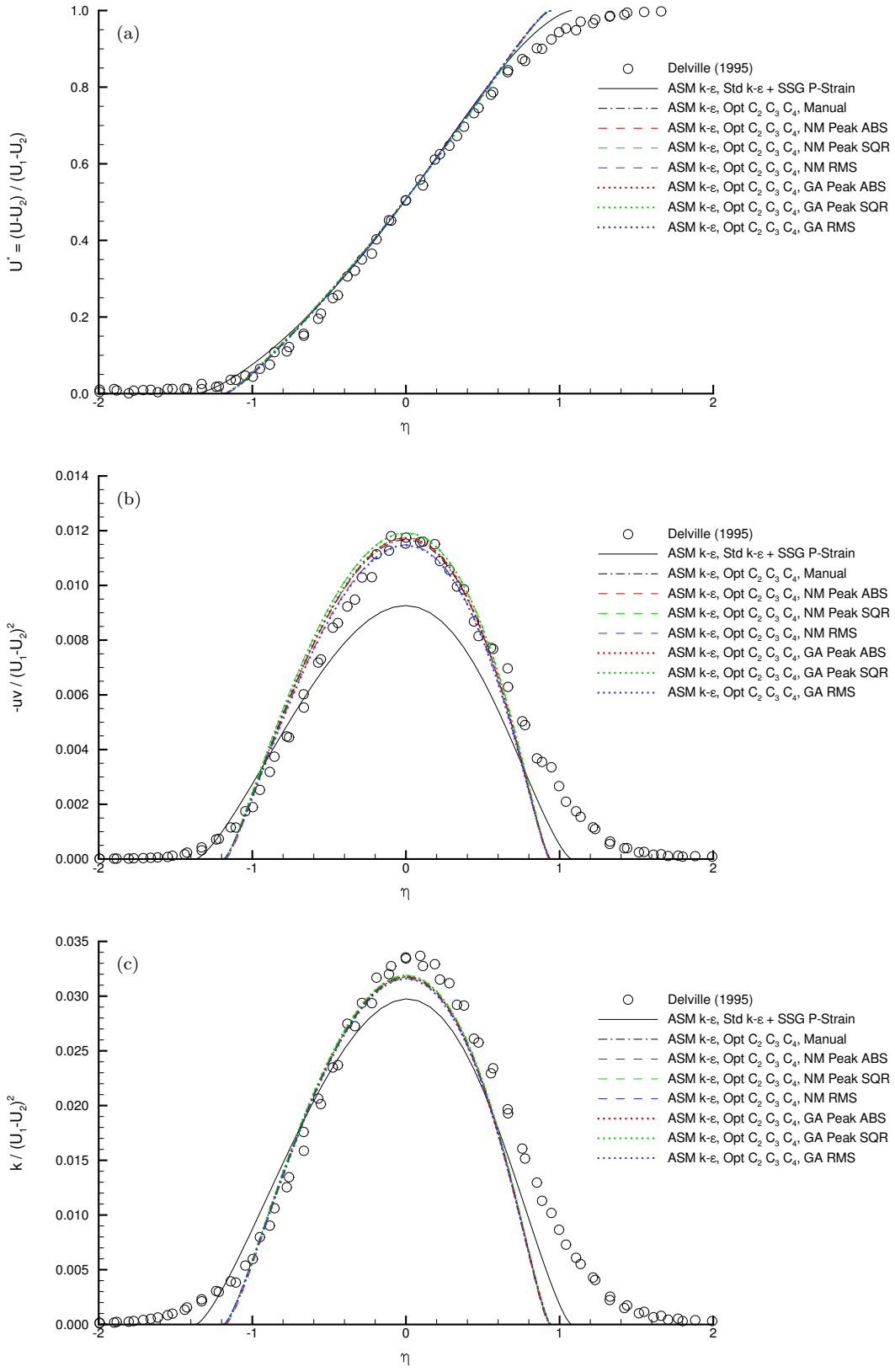

Figure 8: Recalibration study involving the C_2, C_3, and C_4 coefficients.

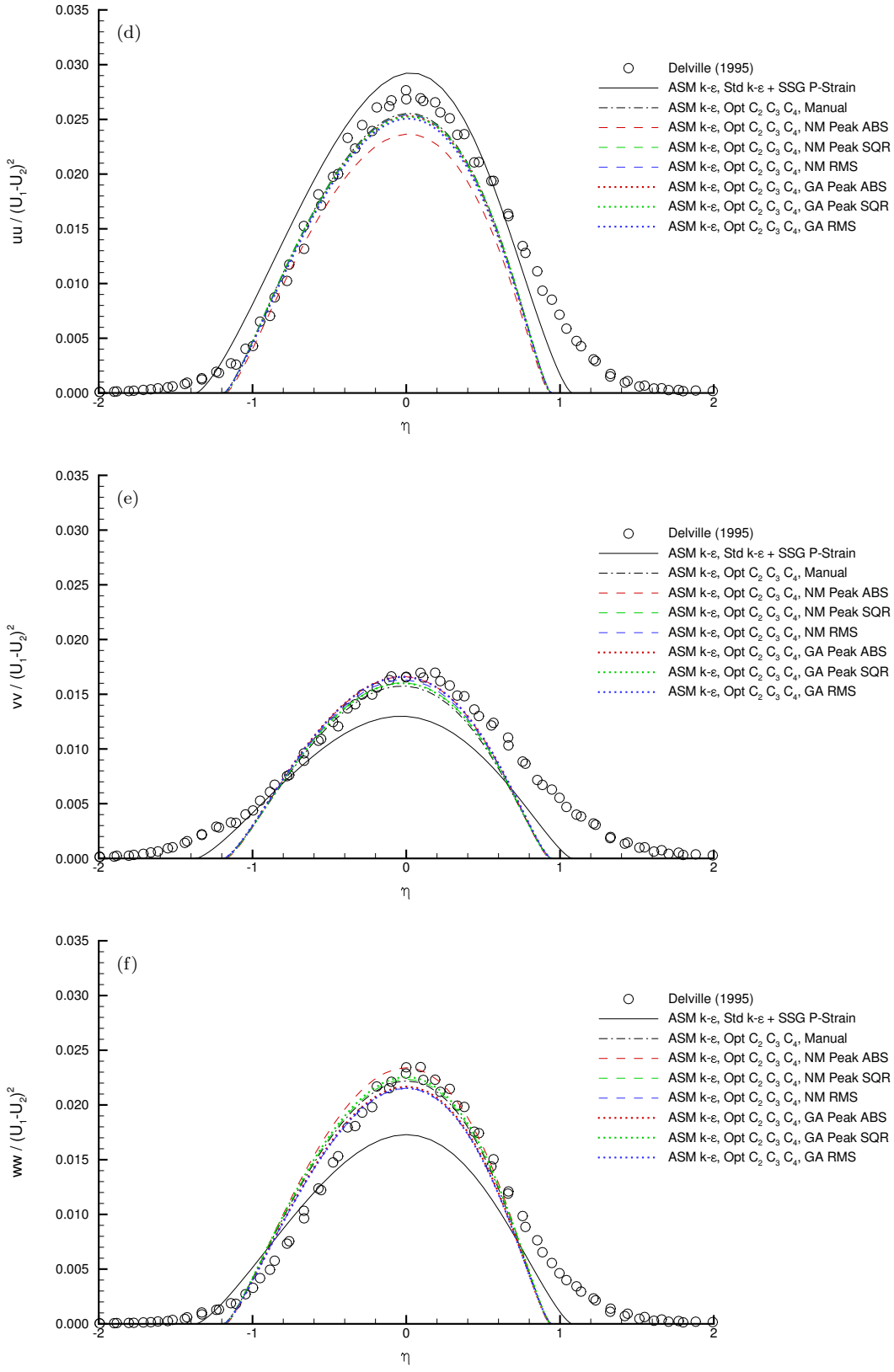

Figure 8: Recalibration study involving the C_2, C_3, and C_4 coefficients (Continued).

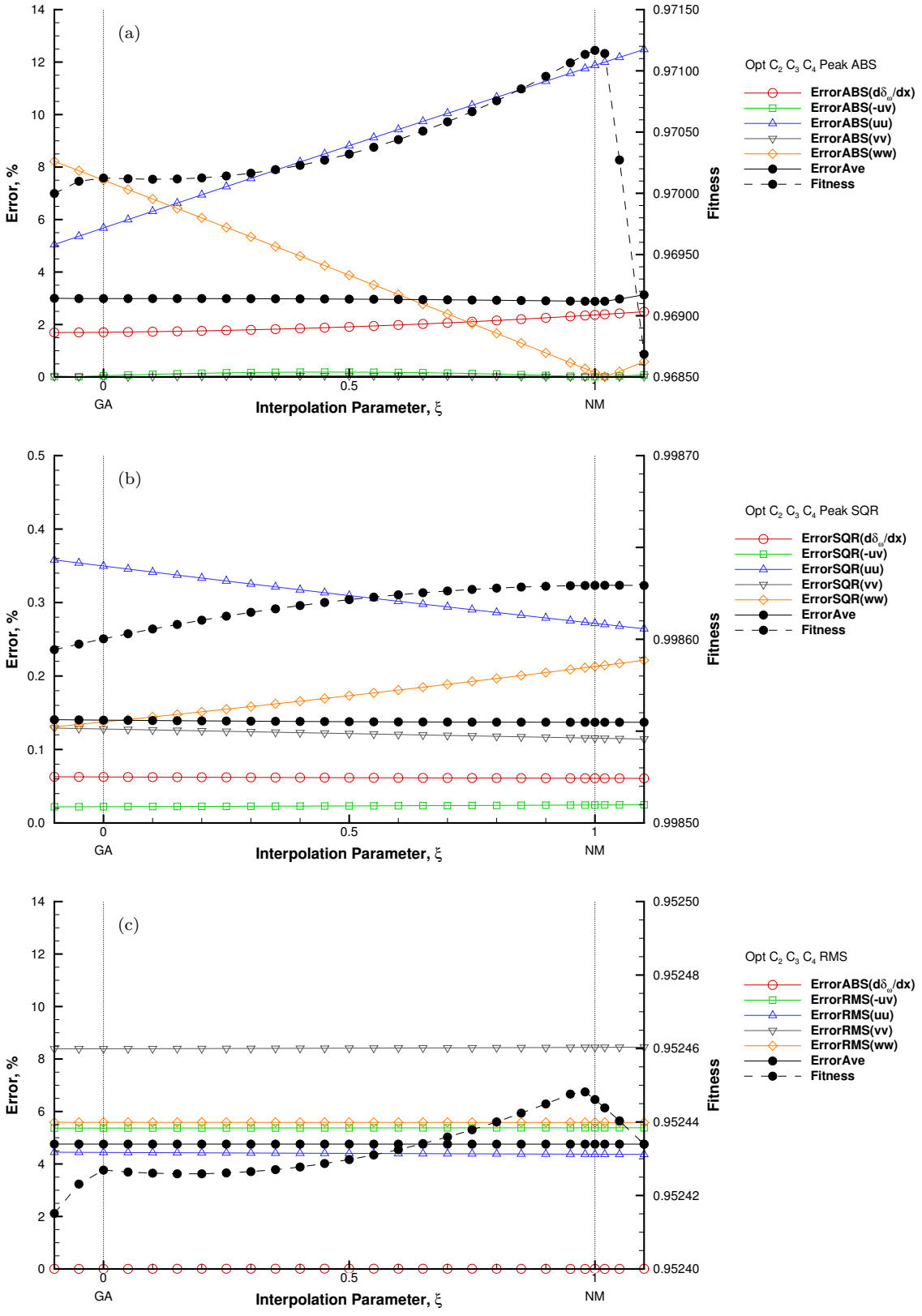

Figure 9: Parametric variation of C_2, C_3, and C_4 coefficients between Genetic Algorithm and Nelder-Mead optima.

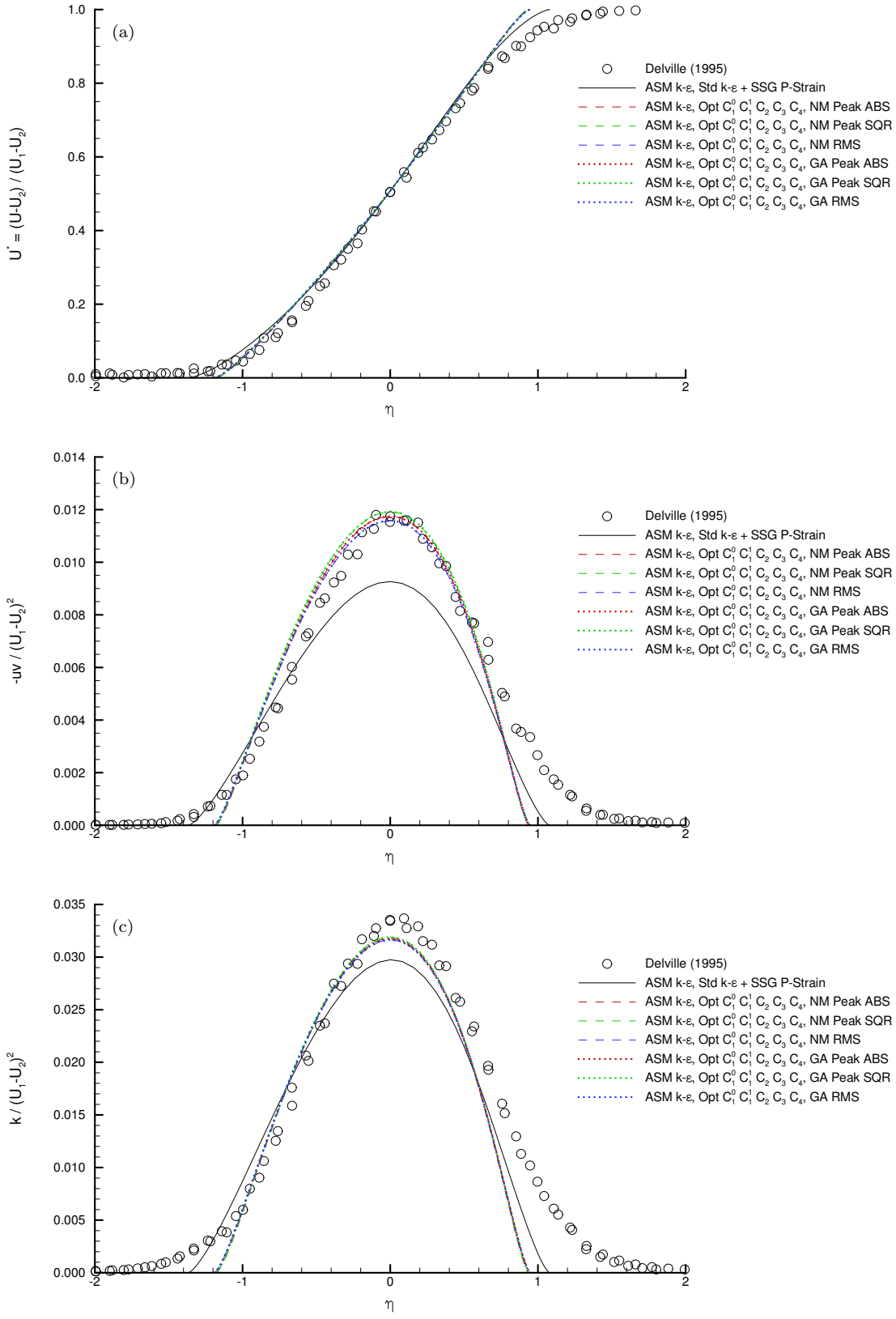

Figure 10: Recalibration study involving the C_1^0, C_1^1, C_2, C_3, and C_4 coefficients.

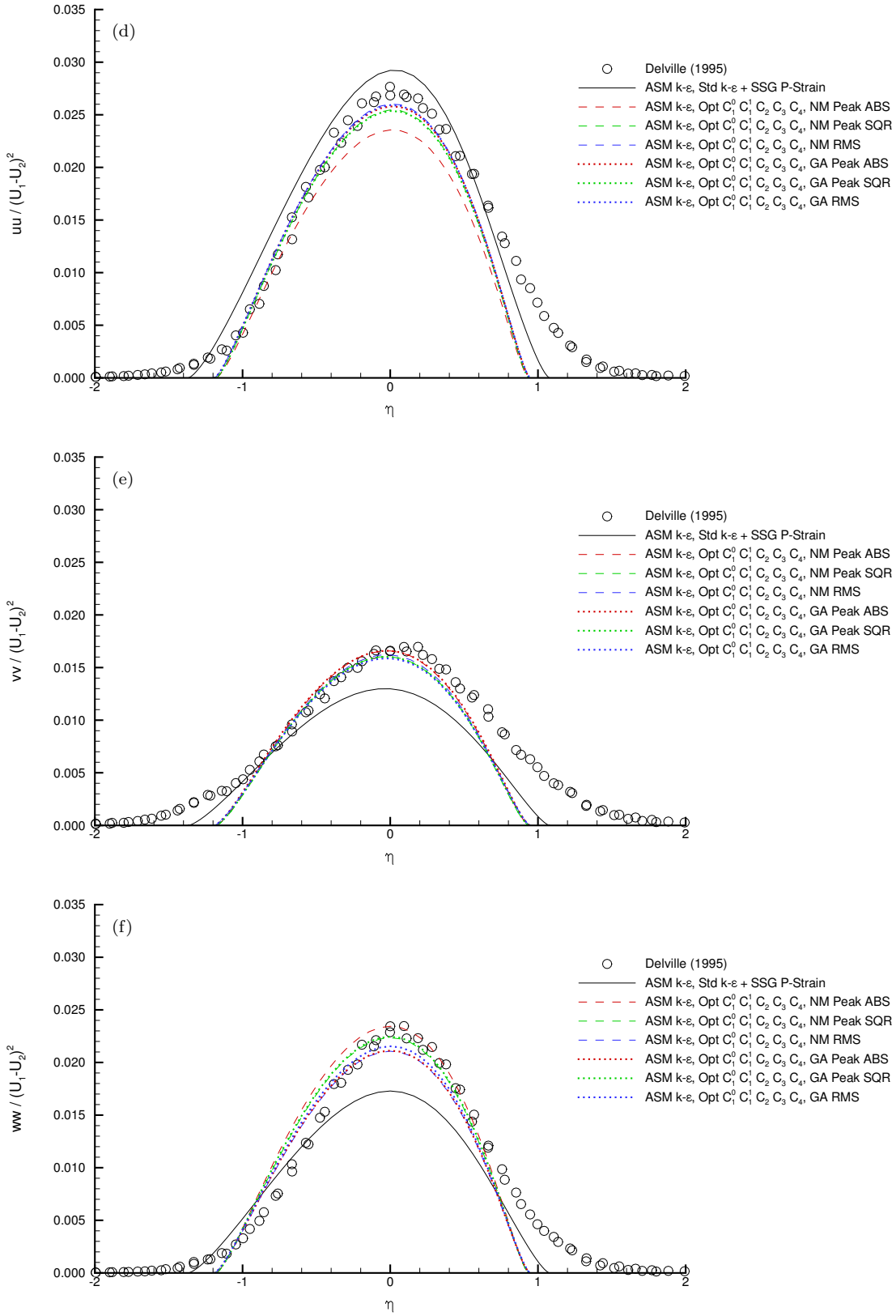

Figure 10: Recalibration study involving the C_1^0, C_1^1, C_2, C_3, and C_4 coefficients (Continued).

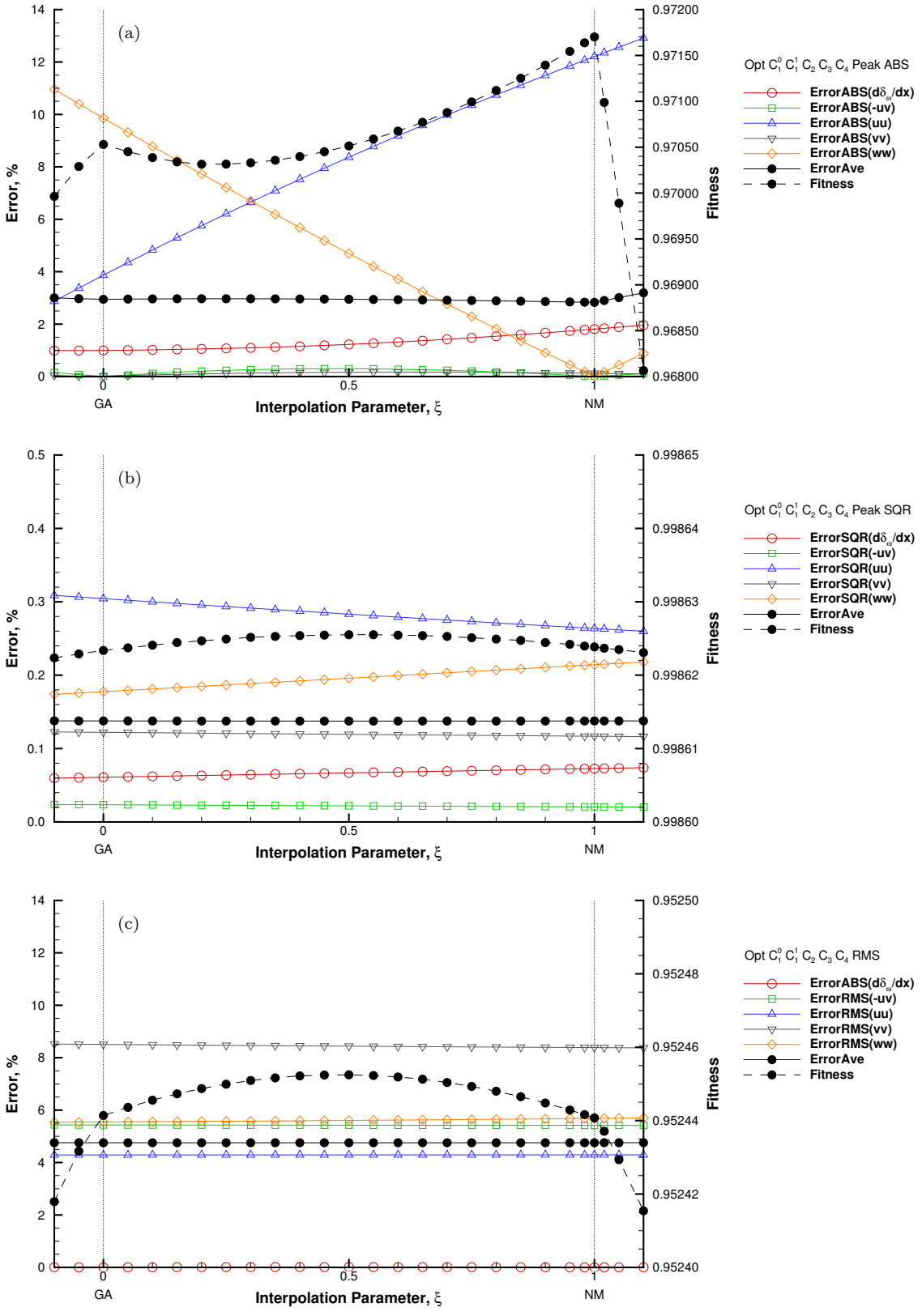

Figure 11: Parametric variation of C_1^0, C_1^1, C_2, C_3, and C_4 coefficients between Genetic Algorithm and Nelder-Mead optima.

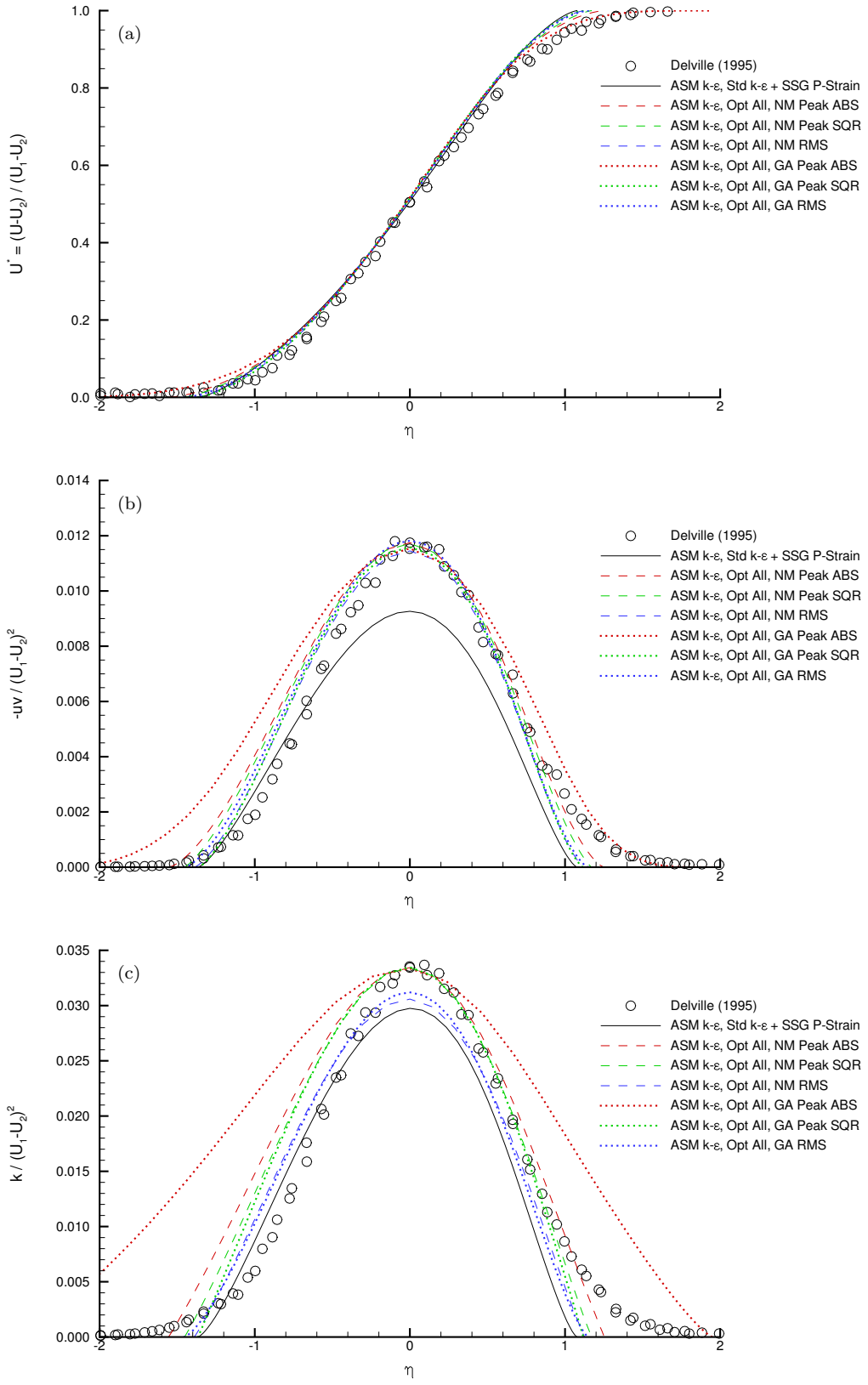

Figure 12: Recalibration study involving all of the k-ϵ and pressure-strain coefficients.

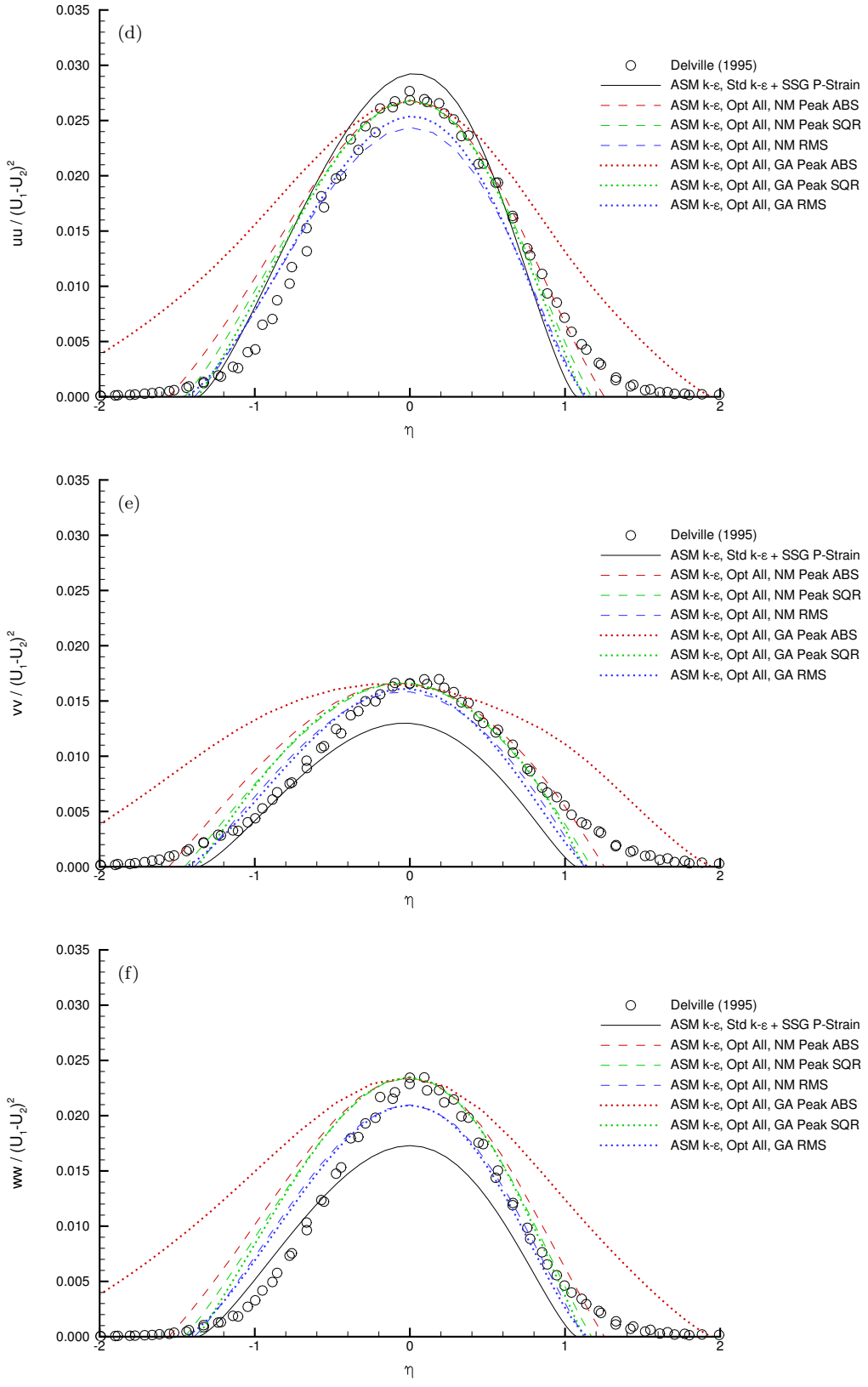

Figure 12: Recalibration study involving all of the k-ϵ and pressure-strain coefficients (Continued).

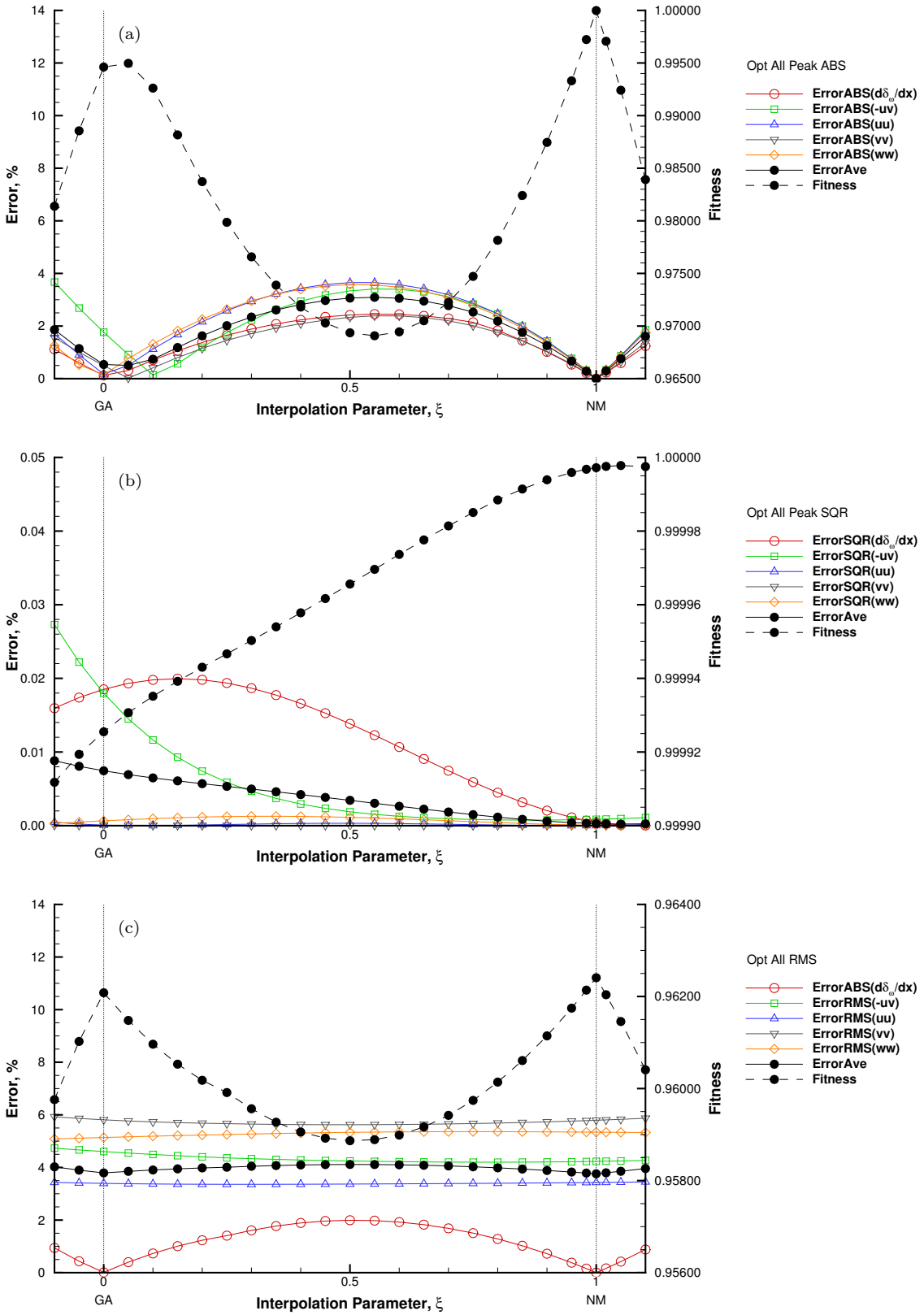

Figure 13: Parametric variation of all coefficients between Genetic Algorithm and Nelder-Mead optima.

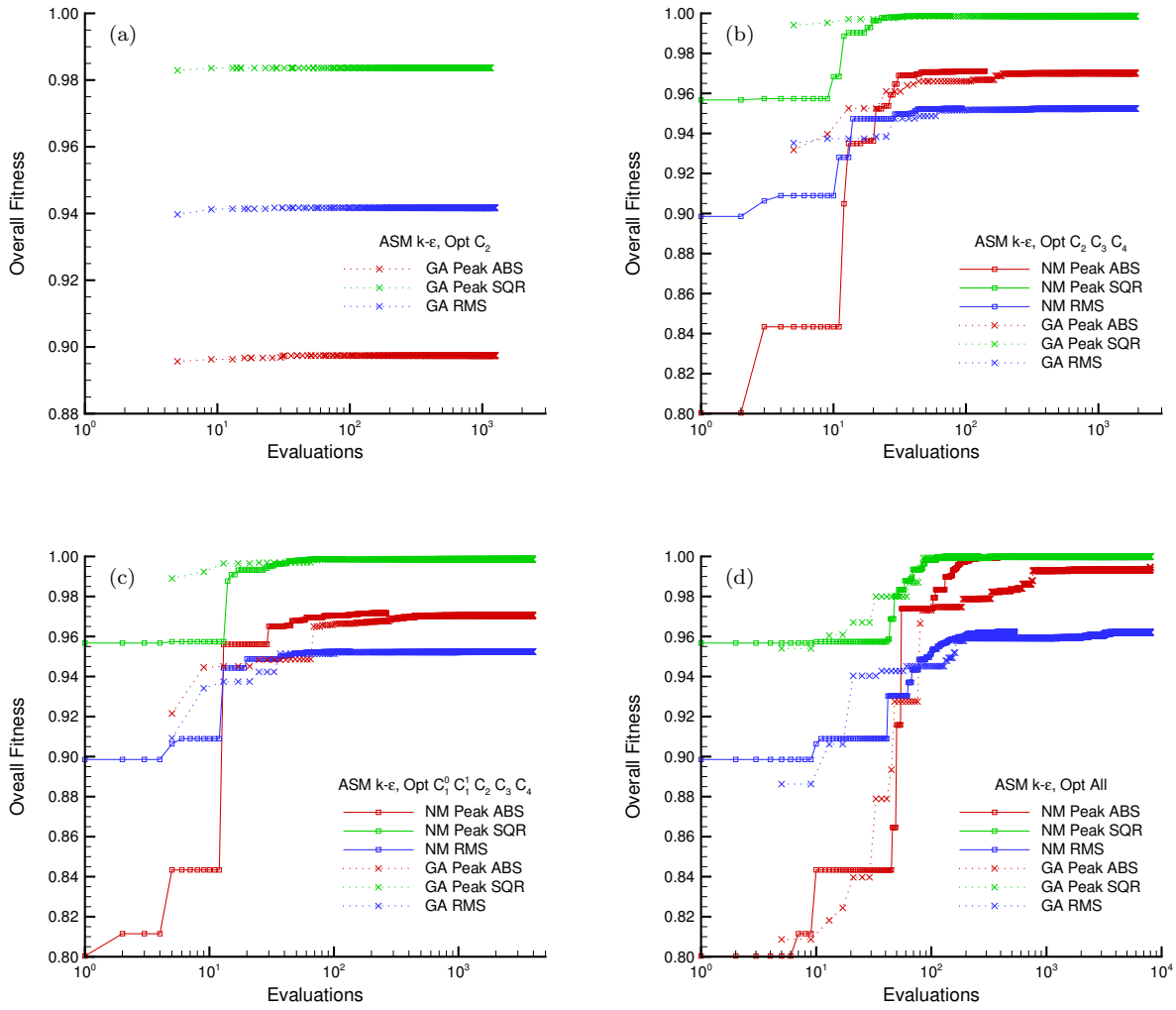

Figure 14: Convergence of optimization methods.

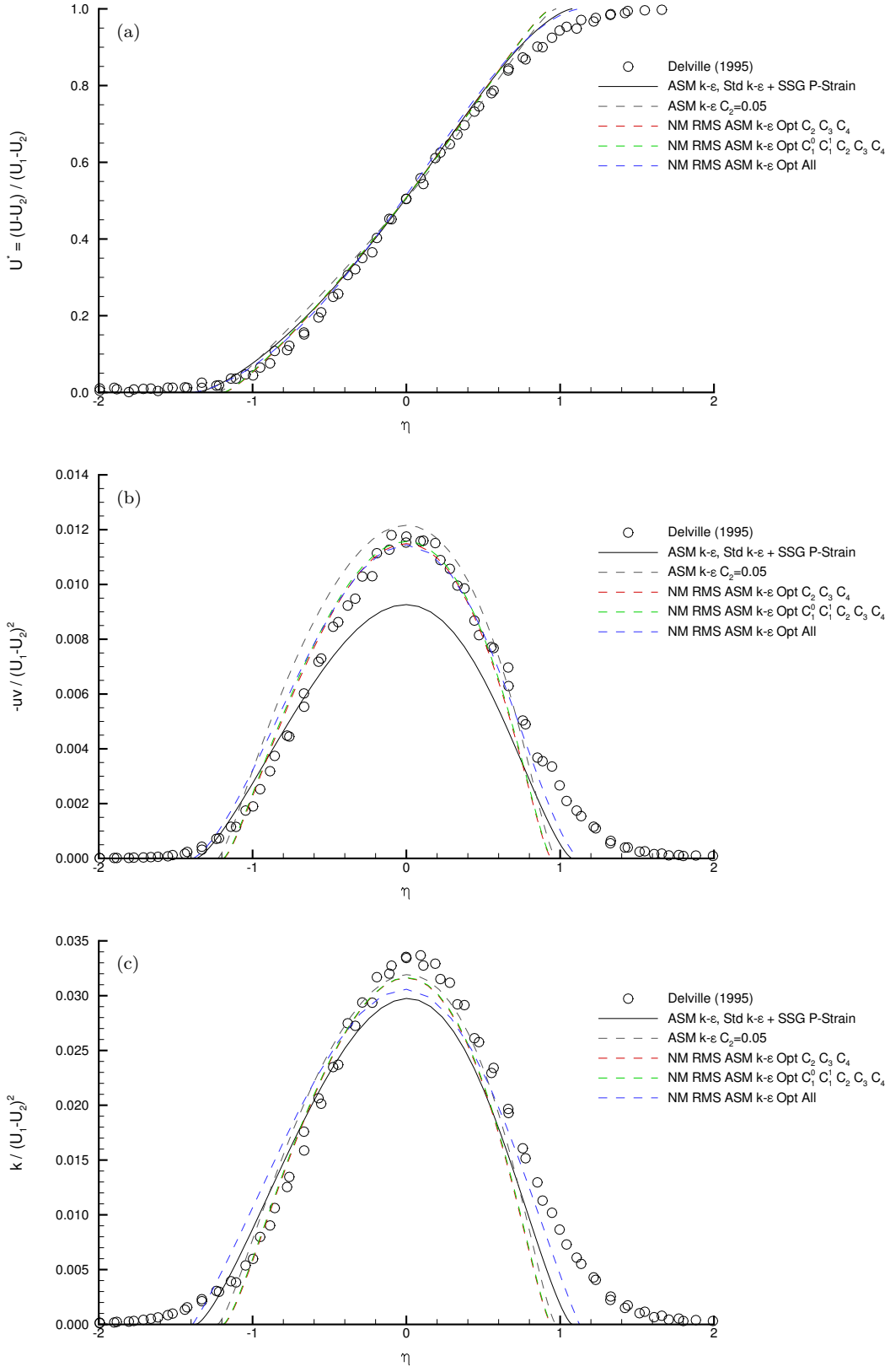

Figure 15: Root-mean-square recalibration studies involving various coefficient sets.

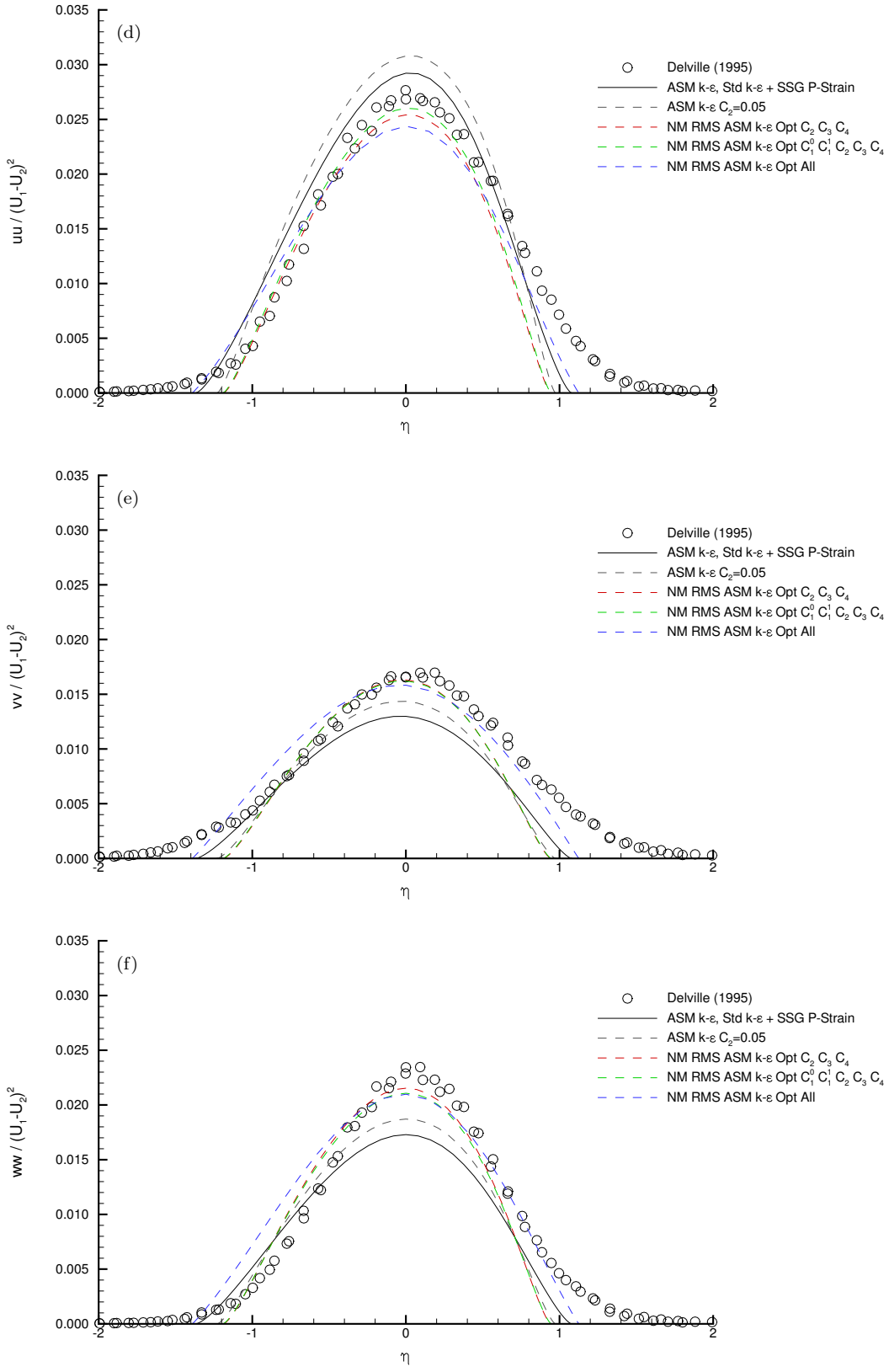

Figure 15: Root-mean-square recalibration studies involving various coefficient sets (Continued).

Model	C_μ	$C_{\epsilon 1}$	$C_{\epsilon 2}$	σ_k	σ_ϵ	C_1^0	C_1^1	C_2	C_3	C_4
Baseline Model										
ASM k-ϵ Std + SSG	0.0900	1.4400	1.9200	1.0000	1.3000	3.4000	1.8000	0.3600	1.2500	0.4000
Hand Opt. ASM k-ϵ										
C_2	0.0900	1.4400	1.9200	1.0000	1.3000	3.4000	1.8000	0.0500	1.2500	0.4000
Nelder-Mead RMS Opt. ASM k-ϵ										
C_2 C_3 C_4	0.0900	1.4400	1.9200	1.0000	1.3000	3.4000	1.8000	0.3984	2.1310	1.1179
C_1^0 C_1^1 C_2 C_3 C_4	0.0900	1.4400	1.9200	1.0000	1.3000	3.7555	2.4154	0.2252	1.9895	0.9103
All Coefs	0.1754	1.4427	2.0117	3.6161	1.9771	0.4043	2.1671	1.1850	2.1671	1.1850

Table 5: Turbulence model coefficients for best optimization.

		Peak Values					Fitness Score		
Case	$d\delta_\omega/dx$	$-uv/\Delta U^2$	$uu/\Delta U^2$	$vv/\Delta U^2$	$ww/\Delta U^2$	$k/\Delta U^2$	Peak ABS	Peak SQR	RMS
Experiment									
Delville Data	0.04995	0.01175	0.02684	0.01660	0.02344	0.03368	1.00000	1.00000	1.00000
Baseline Model									
ASM k-ϵ Std + SSG	0.03910	0.00926	0.02922	0.01298	0.01729	0.02975	0.80035	0.95674	0.89855
Hand Opt. ASM k-ϵ									
C_2	0.04968	0.01216	0.03079	0.01435	0.01871	0.03192	0.89504	0.98360	0.94170
Nelder-Mead RMS Opt. ASM k-ϵ									
C_2 C_3 C_4	0.04995	0.01149	0.02541	0.01630	0.02153	0.03162	0.96501	0.99794	0.95245
C_1^0 C_1^1 C_2 C_3 C_4	0.04995	0.01157	0.02602	0.01621	0.02107	0.03165	0.96593	0.99761	0.95244
All Coefs	0.04995	0.01145	0.02438	0.01583	0.02098	0.03059	0.94633	0.99556	0.96241

Table 6: Incompressible mixing layer results for best optimization.